THE ASTROPHYSICAL JOURNAL SUPPLEMENT SERIES, 117:209–231, 1998 July
© 1998. The American Astronomical Society. All rights reserved. Printed in U.S.A.

MULTIPLE MOLECULAR WINDS IN EVOLVED STARS. I. A SURVEY OF CO(2–1) AND CO(3–2) EMISSION FROM 45 NEARBY ASYMPTOTIC GIANT BRANCH STARS

G. R. KNAPP
Department of Astrophysical Sciences, Princeton University, Princeton, NJ 08544; gk@astro.princeton.edu

K. YOUNG
Harvard-Smithsonian Center for Astrophysics, 60 Garden Street, Cambridge, MA 02138; rtm@dolson.harvard.edu

E. LEE
Department of Astrophysical Sciences, Princeton University, Princeton, NJ 08544; erick@astro.princeton.edu

AND

A. JORISSEN
Université Libre de Bruxelles, C.P. 226, Boulevard de Triomphe, B-1050 Bruxelles, Belgium; ajorisse@astro.ulb.be

Received 1997 September 17; accepted 1998 February 3

ABSTRACT

This paper describes observations of a new phenomenon in evolved mass-losing asymptotic giant branch (AGB) stars: the presence of two winds with different expansion velocities. CO(2–1) and CO(3–2) line emission was observed for 45 AGB stars at high velocity resolution and double winds found in 20% of the sample. Highly asymmetric lines were found in six other stars. The data tentatively suggest that double winds occur when the star undergoes a change (pulsational mode, chemical composition) and that the very narrow components represent the onset of a new phase of mass loss.

Subject headings: radio lines: stars — stars: AGB and post-AGB — stars: mass loss

1. INTRODUCTION

Highly evolved stars on the asymptotic giant branch (AGB) and beyond are surrounded by extensive circumstellar envelopes produced by the copious mass loss that dominates the evolution at this stage. Observations of infrared continuum emission from circumstellar dust and millimeter-wavelength line emission from circumstellar molecules give the mass-loss rates, wind outflow speeds, chemistry and structure of the winds and allow the mass-loss history of the star to be traced. Several extensive data compilations that provide the empirical basis for investigating the mass-loss phenomenon have been made (see, e.g., Loup et al. 1993), and recent reviews include those by Habing (1996) and Olofsson (1996, 1997a, 1997b).

Circumstellar molecules emit both maser and thermal radiation, and the latter is modeled with a fair degree of success by calculating the emission from a spherically symmetric wind expanding at a uniform velocity at a uniform mass-loss rate, with the effective envelope radius determined by molecular photodissociation by the interstellar radiation field (Morris 1980; Mamon, Glassgold, & Huggins 1988; Kastner 1992; Groenewegen 1994). This model predicts simple line shapes; optically thick emission lines are parabolic, while optically thin lines are flat-topped, and the full width of the line at zero power is twice the terminal outflow speed of the wind.

While this model (hereafter called the "steady wind") gives a decent first-order representation of most circumstellar shells, recent, more detailed observations have found many shells that deviate from this simple description:

1. *Bipolar outflows.*—The shells around many mass-losing stars (e.g., VY CMa, AFGL 2688, and OH 231.8+4.2) show flattened, bipolar structure on scales of $\sim 10^{16}$ cm (see, e.g., Olofsson 1997a).

2. *Very fast molecular winds.*—The highest steady wind outflow speeds, up to ~ 40 km s^{-1}, are found from a few supergiant stars such as IRC +10420 and VY CMa (Loup et al. 1993; Knapp et al. 1998b). A small number of stars have, as well as the steady wind component, molecular emission at much higher speeds, in excess of 200 km s^{-1} in the most extreme cases (Cernicharo et al. 1989; Gammie et al. 1989; Young et al. 1992; Jaminet et al. 1992; Alcolea et al. 1996; Knapp, Jorissen, & Young 1997; Sahai & Nyman 1997). The fast winds do not have parabolic line shapes, and it is unlikely that they are produced by constant-velocity outflow. When observed with sufficient angular resolution, fast winds appear to be bipolar and to be flowing from the poles of dense disks or toroids (Neri et al. 1992; Yamamura et al. 1994).

3. *Interrupted mass loss.*—Olofsson et al. (1996) describe observations of detached molecular shells around several carbon stars, which appear to be produced on thermal pulse timescales.

4. *Multiple-velocity and/or nonspherical outflows.*—Margulis et al. (1990) pointed out that not all molecular line profiles from evolved stars are adequately described by the steady wind model; some lines appear to be roughly Gaussian or triangular in shape. Some few of these non-parabolic profiles have since been observed with sufficient angular and/or velocity resolution to demonstrate that they appear to have two or more components, centered at the stellar systemic velocity but with different outflow velocities. Among the stars showing this phenomenon are *o* Cet (Planesas et al. 1990a, 1990b); R Gem, DK Vul, and possibly several other S stars (Sahai & Liechti 1995); X Her (Kahane & Jura 1996), and RS Cnc (Jorissen & Knapp 1998). The profile shapes differ from those seen for stars with fast winds in that both components have roughly parabolic shapes and the outflow speeds lie within the range (3–30 km s^{-1}) observed for the large majority of evolved stars. These stars thus appear to have *two* steady winds.

Recent improvements in receiver sensitivity, frequency coverage, frequency resolution, and baseline stability make it feasible to carry out low-noise, high velocity resolution observations of a significant sample of circumstellar envelopes to investigate the frequency of occurrence of the multiple wind phenomenon and how it is related to the stellar chemistry, mass-loss rate, and evolutionary stage. This paper begins the discussion and analysis of a series of observations made to investigate multiple slow molecular winds in circumstellar envelopes.

2. OBSERVATIONS

This paper describes observations of the CO(2–1) and CO(3–2) lines made with the 10.4 m Robert B. Leighton telescope of the Caltech Submillimeter Observatory on Mauna Kea, Hawaii. The stars to be observed were selected from large surveys of CO emission (Margulis et al. 1990; Nyman et al. 1992; Loup et al. 1993; Knapp et al. 1998b) as having strong CO line emission, i.e., brighter than about 1 K as observed with a 10 m telescope. We also confined the observations to stars north of about $-30°$ because of the significant atmospheric opacity at submillimeter wavelengths. We can therefore expect to make observations with a high signal-to-noise ratio at high velocity resolution in a reasonable amount of observing time (2 hr or less). The observations were mostly carried out in the period 1996 December 28 to 1997 January 2, when we observed almost all CO-bright stars in the right ascension range available at that time of year, about 23^h to 10^h. The observed sample also contains several stars with weaker CO emission that were observed to fill empty places in the schedule and a small number of observations of stars in other parts of the sky obtained in the previous 2 years, during test and engineering time. The sample of stars described in this paper is thus very incomplete in terms of sky coverage, and we plan to complete these observations in future observing sessions.

In all, high velocity resolution and (mostly) high signal-to-noise ratio observations were obtained for 43 stars, which are listed in Table 1. Table 1 also contains data for two additional stars, both of which are known from previous observations to have double outflows: *o* Ceti (Planesas et al. 1990a, 1990b; Knapp et al. 1998a) and π^1 Gru (Sahai 1992). The CO(2–1) observations of RS Cnc are from Jorissen & Knapp (1998).

Table 1 lists the star's most common name, the observed position, the spectral type, the variable type, the basic chemistry (O = oxygen rich, C = carbon star, S = S star), the period where known, and a simple classification for the shape of the CO line profile (see below).

Most of the spectral types and chemistry classes are from Loup et al. (1993) or from the SIMBAD listings. Most of the variable types and periods are from the Catalogue of Variable Stars by Kholopov et al. (1985); the period of 55^d listed in that catalog for EP Aqr is uncertain. The periods for several stars with thick circumstellar shells (R Scl, R Lep, AFGL 865, AFGL 971, IW Hya, IRC +10216, and IRC +40540) are given by Le Bertre (1992, 1993) and Cohen & Hitchon (1996). The period of the post-AGB carbon star HD 56126 is from Lèbre et al. (1996). Several of the variable types in the fifth column are from Kerschbaum & Hron (1992, 1994); these authors show that the semiregular SRa class (Kholopov et al. 1985) contains a mixture of Mira and SRb (hereafter "true" semiregular variables) and have reclassified several stars; R Scl from SRa to SRb and BK Vir and π^1 Gru from Lb (cool irregular variable; see Kerschbaum, Lazaro, & Harbison 1996) to SRb.

The molecular line observations were made in either the CO(2–1) or the CO(3–2) line depending on the weather, which was variable during the observing run. The observations were made using liquid-helium–cooled SIS junction receivers with double-sideband system temperatures of $\sim$100 K and 130 K at 230 and 345 GHz. The telescope half-power beamwidths are 30″ and 20″ at these frequencies, and the main-beam efficiencies are 76% and 65%. The receivers for both frequency bands are double sideband, and spectral lines in the image sideband, 3 GHz below the observed frequency for both receivers, were also detected.

The spectral lines were observed by three acousto-optic spectrographs (AOS), with bandwidths of 1.5 GHz over 2048 channels, 500 MHz over 1024 channels, and 50 MHz at 1024 channels. The velocity resolution of the 50 MHz AOS is $\sim$0.12 km s^{-1} at 345 GHz and $\sim$0.2 km s^{-1} at 230 GHz. The spectrometer frequency was calibrated using an internally generated frequency comb, and the velocity scale is corrected to the local standard of rest (LSR).

The observations were made by chopping between the star position and an adjacent sky position with the secondary mirror, using a chop throw of 120″ in azimuth at a rate of 1 Hz. Pairs of chopped observations were made with the source placed alternately in each beam. The spectral baselines resulting from this procedure are linear to within the rms noise for all bandwidths with a small number of exceptions for which the 500 MHz data show small (0.005–0.01 K) baseline nonlinearities. The CO emission from all of the observed stars is strong enough that it was used to measure the telescope pointing offsets before each observation.

The temperature scale and the atmospheric opacity were measured by comparison with a hot (room temperature) load. The line temperature was corrected for the main-beam efficiency, and the resulting scale is the Rayleigh-Jeans equivalent main-beam brightness temperature, $T_{\rm MB}$, i.e., that measured by a perfect 10.4 m antenna above the atmosphere. The high velocity resolution CO line profiles are shown in Figure 1.

Most of the line profiles are closely approximated by parabolic or flattened parabolic shapes (e.g., AFGL 865 and W Aql). These line profiles are classified in Table 1 as parabolic, P. The CO(2–1) line profiles for IRC +10216 and χ Cyg show a small blueshifted feature that can be attributed to radiative transfer effects in a shell with a monotonically decreasing radial temperature gradient and a small amount of turbulence (Huggins & Healy 1986). Two of the profiles, those for AFGL 971 and V Cyg, are affected by Galactic emission, and hence their profile shapes are uncertain. There is strong Galactic emission near 0 km s^{-1} in the "on" and "off" positions seen in the broadband profile of IRC +60144 that may affect the observed line shape. All three line profiles are classified as parabolic. The observations of several other stars (R And, S CMi, S Vir, V CrB, and R Ser) were made with insufficient signal-to-noise ratio to measure the profile shape and are classified as parabolic by default. Uncertain classifications are enclosed in parentheses.

Several line profiles are distinctly nonparabolic. Most striking are those showing two winds, i.e., two components of different width centered at the same velocity; examples are IRC +50049, X Her, and EP Aqr. These are classified as D, or double-wind profiles. Several other stars, e.g., R Scl and R Leo, have asymmetric line profiles, with one side of the profile being brighter than the other. These are classified

TABLE 1

OBSERVED STARS

Star	α (1950)	δ (1950)	Spectral Type	Variable Type	Chemistry	P (days)	Profile[a]
IRC +40004	00 04 17.7	+42 48 18	M10	Mira	O		P
R And	00 21 23.0	+38 18 02.3	S4, 6e	Mira	S	409	(P)
R Scl	01 24 40.02	−32 48 06.8	C6, 4	SRb	C	370	A/Blue
IRC +50049	01 55 37.3	+45 11 31.9	M8		O		D
o Cet	02 16 49.04	−03 12 13.4	M7e	Mira	O	332	D[b]
IRC +50096	03 22 59.1	+47 21 22.0	C	Mira	C	540	P
IRC +60144	04 30 45.9	+62 10 12			C		(D)[c]
TX Cam	04 56 40.6	+56 06 28	M8.5	Mira	O	557	P
R Lep	04 57 19.7	−14 52 47.5	C7, 4e	Mira	C	433	P
α Ori	05 52 27.8	+07 23 57.9	M2 Iab	SRc	O	2070	A/Blue
U Ori	05 52 51.0	+20 10 06.2	M8	Mira	O	372	P
AFGL 865	06 01 17.4	+07 26 06.0		Mira	C	696	P
AFGL 971	06 34 16.5	+03 28 04.0		Mira	C	653	(P)[c]
GX Mon	06 50 03.5	+08 29 02	M9	Mira	O	527	P
R Gem	07 04 20.78	+22 46 56.7	S3, 9e	Mira	S	370	D
HD 56126	07 13 25.3	+10 05 09.2	F5 Iab:		C	27	P
S CMi	07 30 00.3	+08 25 35.5	M7e	Mira	O	332	(P)
RS Cnc	09 07 37.7	+31 10 05	M6se	SRc?	S	120	D
R LMi	09 42 34.7	+34 44 34.3	M7e	Mira	O	372	A/Red
IW Hya	09 42 56.4	−21 47 53.6	M9	Mira	O	636	P
R Leo	09 44 52.2	+11 39 41.9	M8e	Mira	O	313	A/Red
IRC +10216	09 45 14.89	+13 30 40.8	C9, 5	Mira	C	637	P
U Hya	10 35 05.0	−13 07 26.2	C6, 4	SRb	C	450	P
R Crt	10 58 06.0	−18 03 21.8	M7	SRb	O	160	P
BK Vir	12 27 48.1	+04 41 34.5	M7	SRb	O		P
Y UMa	12 38 04.4	+56 07 14.8	M7	SRb	O	168	P
Y CVn	12 42 47.08	+45 42 47.9	C5, 5J	SRb	C	158	P
RT Vir	13 00 05.7	+05 27 15.2	M8	SRb	O	155	P
SW Vir	13 11 29.75	−02 32 32.6	M7	SRb	O	150	A/Red
R Hya	13 26 58.48	−23 01 24.5	M6.5e	Mira	O	388	D
S Vir	13 30 23.2	−06 56 18.1	M7e	Mira	O	378	(P)
W Hya	13 46 12.2	−28 07 06.5	M8e	SRa	O	382	P
RX Boo	14 21 56.7	+25 55 48.5	M7.5	SRb	O		P
S CrB	15 19 21.53	+31 32 46.5	M7e	Mira	O	360	P
V CrB	15 47 44.08	+39 43 22.7	C6, 2e	Mira	C	358	(P)
R Ser	15 48 23.2	+15 17 02.7	M6.5e	Mira	O	357	(P)
X Her	16 01 08.8	+47 22 35.8	M6	SRb	O	95	D
RU Her	16 08 08.6	+25 11 59	M7e	Mira	O	485	P
W Aql	19 12 41.68	−07 08 08.4	S3, 9	Mira	S	490	P
χ Cyg	19 48 38.48	+32 47 11.8	S7, 2e	Mira	S	407	P
V Cyg	20 39 41.32	+47 57 45.4	C5, 3e	Mira	C	421	P[c]
EP Aqr	21 43 56.46	−02 26 40.9	M8	SRb	O	55	D
π^1 Gru	22 19 41.13	−46 12 02.4	S5, 7	SRb	S		D[d]
IRC +40540	23 32 01.3	+43 16 27	C8, 3.5		C	628	P
R Cas	23 55 51.7	+51 06 36.4	M7e	Mira	O	431	A/Red

NOTE.—Units of right ascension are hours, minutes, and seconds, and units of declination are degrees, arcminutes, and arcseconds.

[a] P: parabolic. D: double; two distinct components centered at the same velocity with different outflow velocities. A: asymmetric, with red or blue emission wings. Classifications in parentheses are for profiles with low signal-to-noise ratio, significant Galactic contamination, or uncertain classification.

[b] CO profile classification from data given by Planesas et al. 1990a, 1990b and Knapp et al. 1998a.

[c] CO profile affected by Galactic emission.

[d] CO profile classification from data given by Sahai 1992.

REFERENCES.—Periods for R Scl, R Lep, AFGL 865, and AFGL 971 from Le Bertre 1992. Period for IRC +50096 from Jones et al. 1990. Period for HD 56126 from Lèbre et al. 1996. Period for IW Hya from Le Bertre 1993. Period for IRC +10216; mean of periods from Le Bertre 1992 and Cohen & Hitchon 1996. Period of IRC +40540 from Cohen & Hitchon 1996.

as A (for asymmetric) Blue or Red, depending on whether the red or blue side of the profile is stronger. The possible origin of these line profile shapes will be discussed elsewhere. The stars with asymmetric profiles will be included in the group with parabolic line profiles in the discussion below, where stars in this combined group are compared with those with double winds.

In almost all cases of stars with double winds, the narrow component has a similar width to the emission lines from interstellar molecular clouds—compare the observations of the contaminated profile of AFGL 871 and of the double-wind profile for EP Aqr in Figure 1. Are these double-wind line profiles, then, simply an artifact of superimposed emission from molecular clouds? We believe not, for the following reasons. First, mapping observations of several of these stars, *o* Cet (Planesas et al. 1990a, 1990b), RS Cnc (Neri et al. 1997), X Her (Kahane & Jura 1996), π^1 Gru (Sahai 1992), and EP Aqr (Knapp, Young, & Sahai 1998c), show that both the broad and narrow components are colocated, centered on the star and of small angular extent. Second, the central velocities of both the broad and the narrow components are closely the same (see Table 2 below). We there-

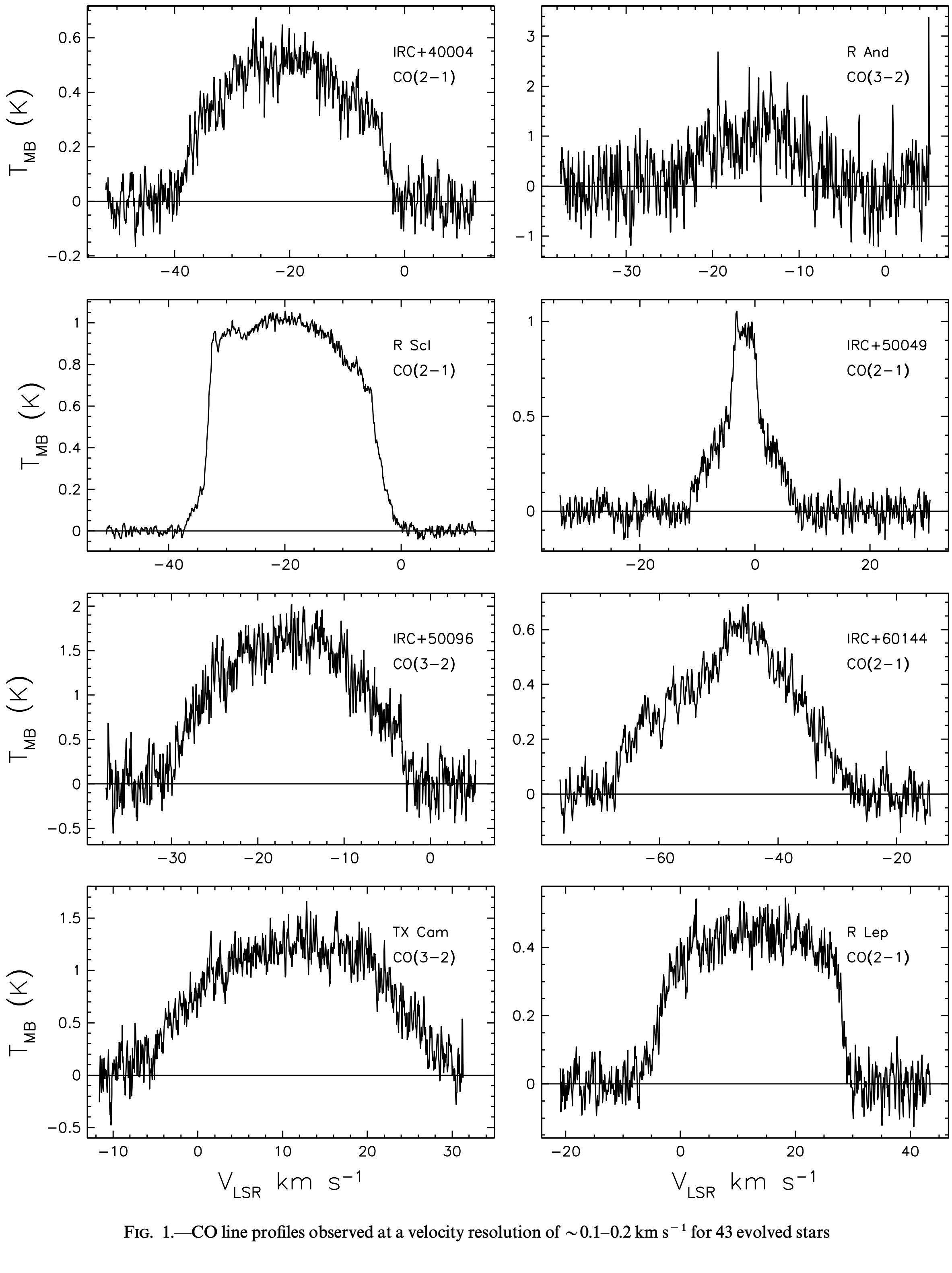

FIG. 1.—CO line profiles observed at a velocity resolution of ~ 0.1–$0.2\ \mathrm{km\ s^{-1}}$ for 43 evolved stars

fore have high confidence that both the broad and narrow components observed in the emission profiles represent circumstellar gas produced by mass loss.

How well can the presence of double winds be found in these observations? A series of simulated CO(2–1) line profiles, with two components centered on the same velocity but with different outflow velocities, was constructed to investigate this question (for details, see § 4.3 below). In all cases, the fast wind component has an outflow speed $V_f = 10\ \mathrm{km\ s^{-1}}$ and a mass-loss rate of $3 \times 10^{-7}\ M_{\odot}\ \mathrm{yr^{-1}}$. The model envelope was assumed to be at a distance of 200 pc and to be observed with the CSO 10.4 m telescope; the resulting spectral line is parabolic with a peak temperature of $T_f = 0.65$ K. The models were calculated with a velocity resolution of $0.1\ \mathrm{km\ s^{-1}}$, an rms noise of 0.4 K, and flat baselines.

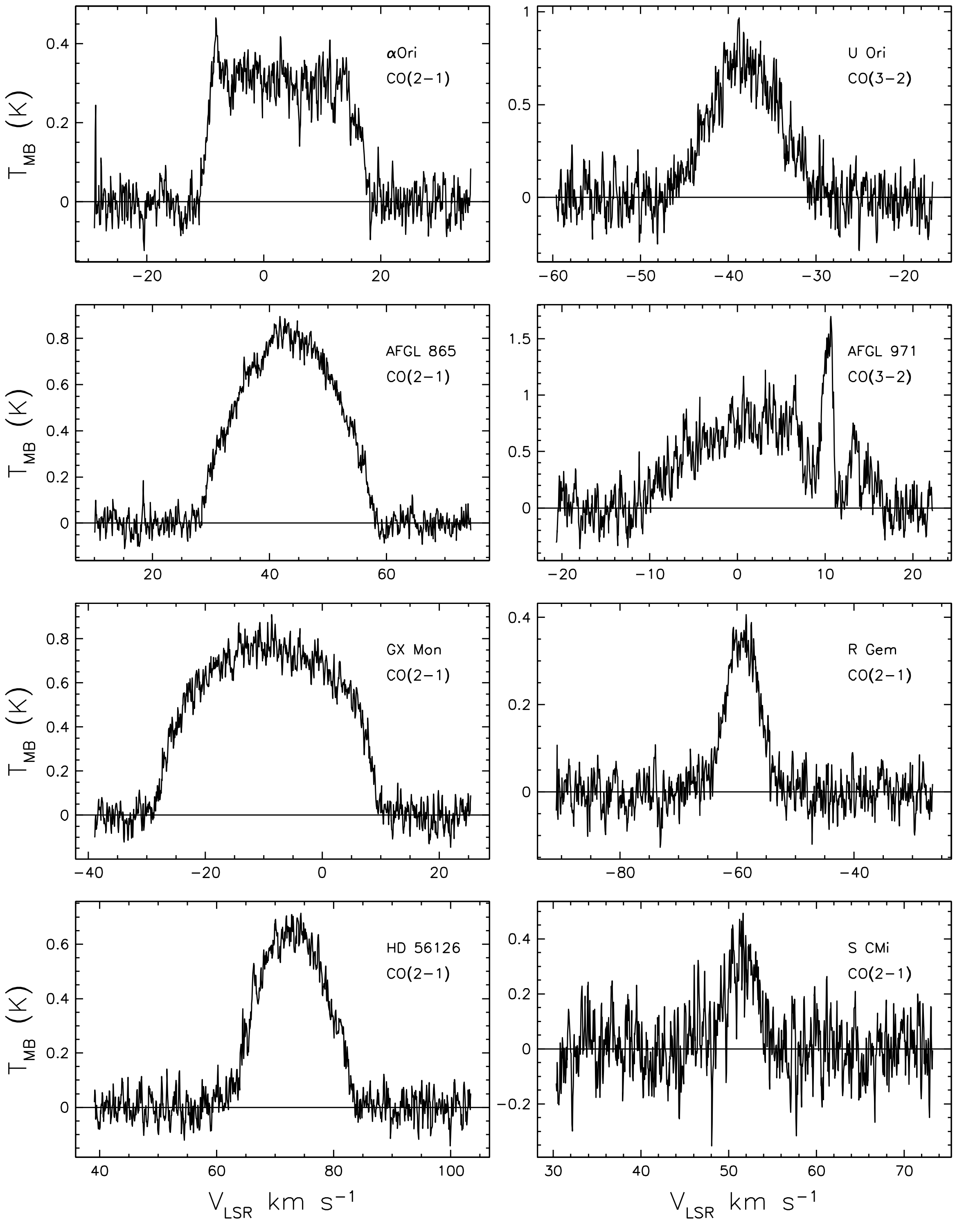

FIG. 1.—*Continued*

A second component was then added, with varying peak temperature T_S and outflow speed V_s. These simulations showed the following:

1. If $V_s/V_f > 0.7$, the resulting line profile is sufficiently parabolic in shape that the presence of two winds cannot be distinguished.
2. If $0.7 < V_s/V_f < 0.5$, the presence of the two winds can be seen in a high-quality line profile provided $T_s \sim T_f$.
3. If $V_s/V_f < 0.5$, the slow wind can always be distinguished provided that T_s is greater than 5 times the rms noise.

A selection of the simulated profiles is shown in Figure 2.

The bottom line is that we can reliably detect a double wind only when there is a reasonable contrast between the fast and slow winds, i.e., when the outflow velocities differ by a factor of 2 or more. We therefore cannot use the data in

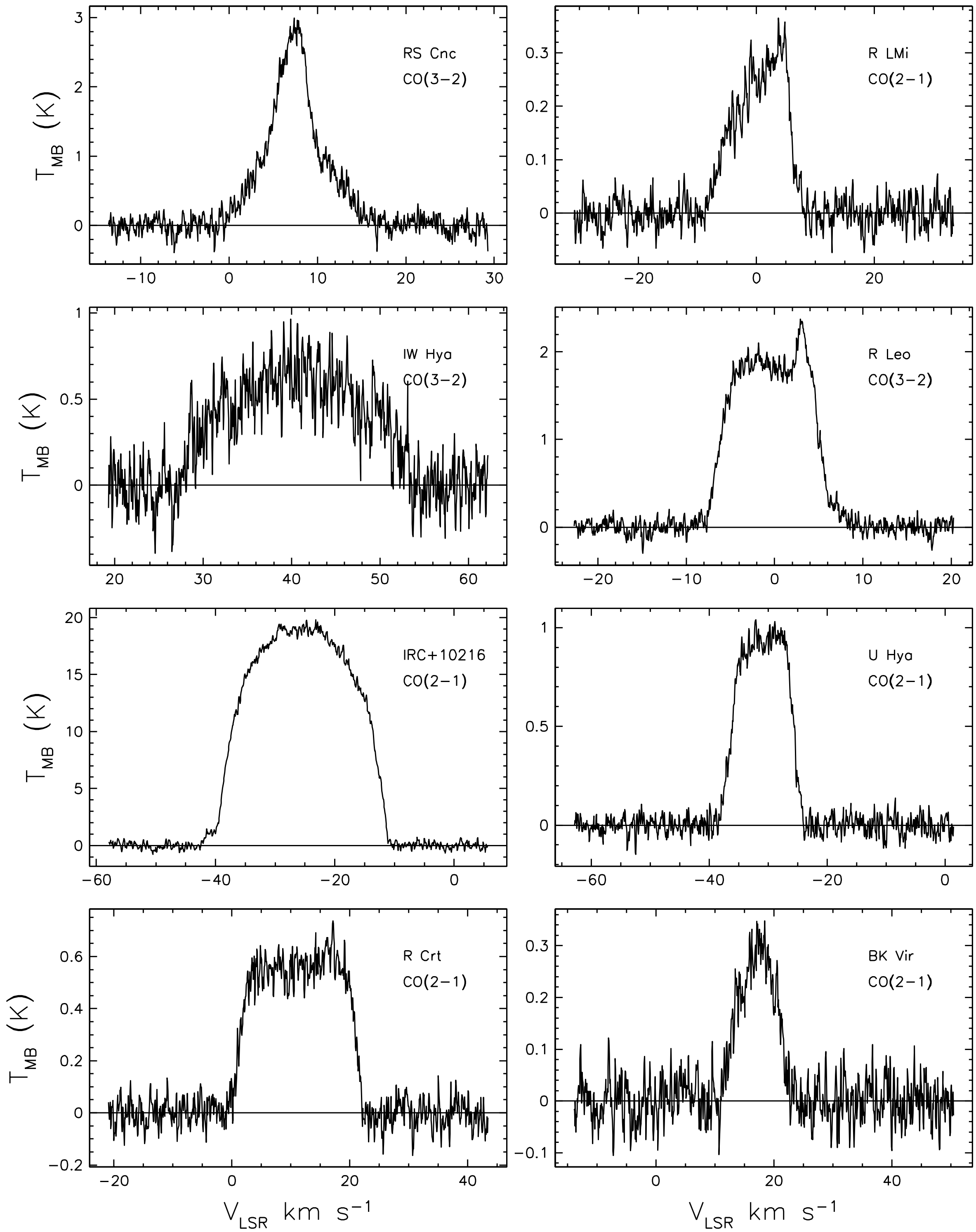

FIG. 1.—*Continued*

this paper to rule out the possibility that *all* stars have multiple winds with similar expansion velocities. This caution applies to all of the discussion and conclusions in the remainder of this paper. It is of interest in this context that high spatial resolution far-infrared maps of two of the carbon stars in Table 1, U Hya and Y CVn, find double/detached shells (Waters et al. 1994; Izumiura et al. 1996) but the global CO line profiles for these stars (Fig. 1) show no discernible velocity structure.

3. LINE PROFILES AND STELLAR PROPERTIES

3.1. *Chemistry*

Table 1 lists 45 stars: 26 are oxygen-rich, six are S stars, and 13 are carbon stars. Six of the stars have asymmetric profiles, and all of these save R Scl are oxygen-rich. Nine of the stars have double profiles: three of these are S stars, one is a carbon star, and five are oxygen stars; however, the presence of a narrow component for the carbon star IRC

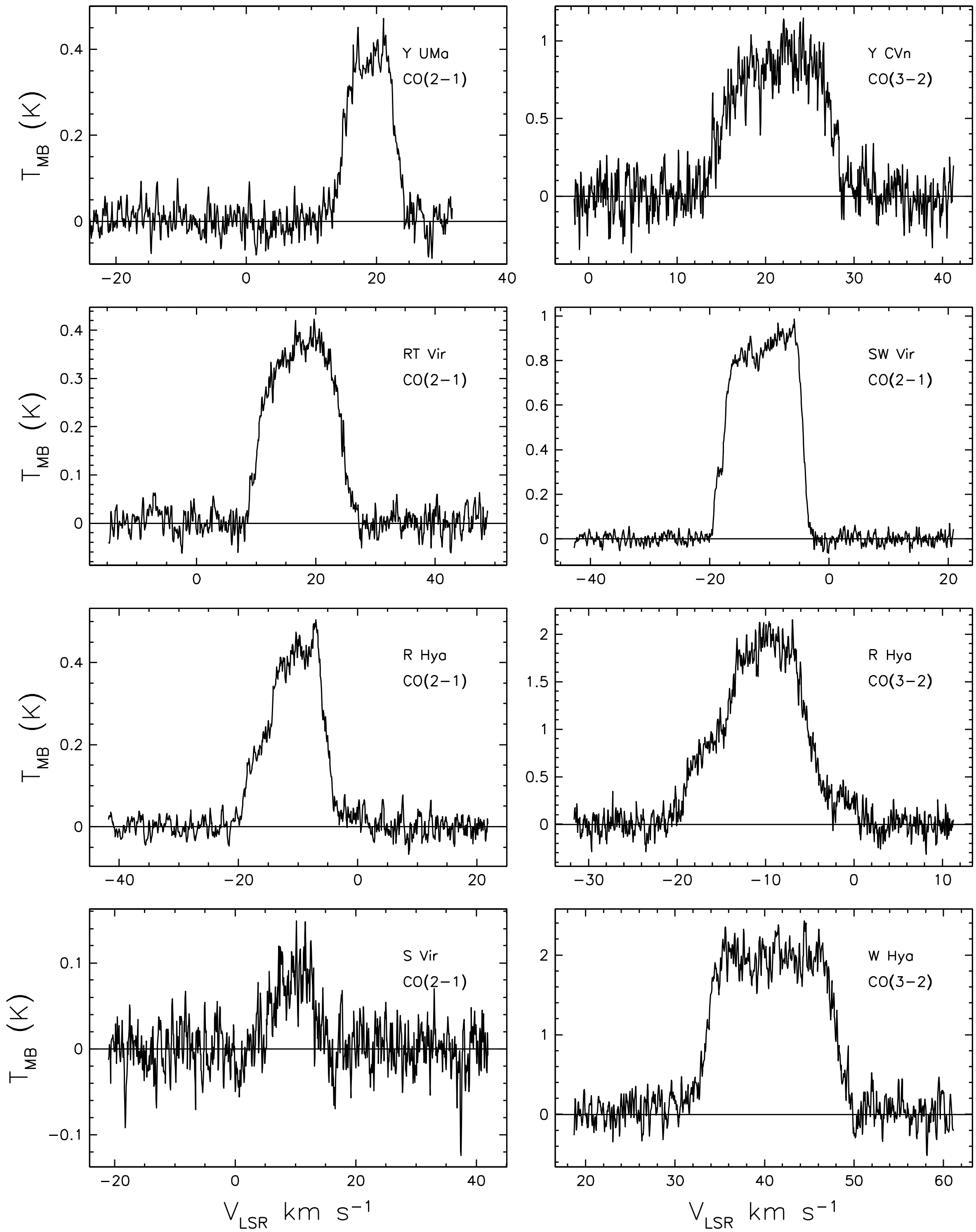

FIG. 1.—*Continued*

+60144 is somewhat uncertain (see Fig. 1). The remainder have parabolic line profiles (and a few are observed with insufficient sensitivity to define the line shape well.) Thus, at least 38% of the oxygen stars, 50% of the S stars, and 15% of the carbon stars have nonparabolic line profiles. These results show the trend noted by Margulis et al. (1990); the line profiles from oxygen-rich circumstellar envelopes have more structure than do those for carbon-rich envelopes.

3.2. *Pulsational Properties*

Figure 3 shows the histogram of the periods of stars with double and with parabolic line profiles; the former tend to have shorter periods. This difference is also apparent when variable type is considered; most (20) of the 26 Mira variables have parabolic profiles, while only half of the 15 SR variables do. Further, while the period distribution of the

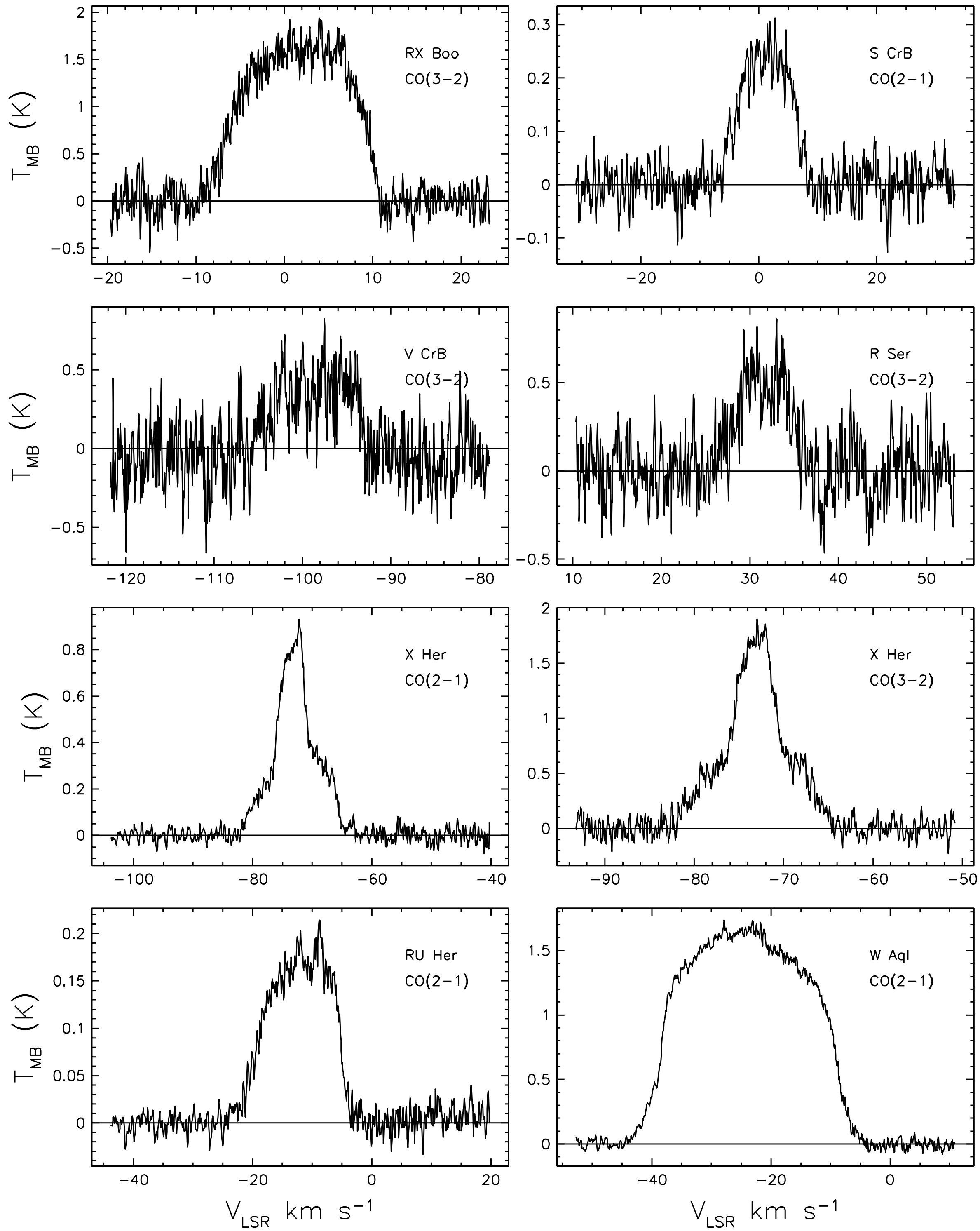

FIG. 1.—*Continued*

whole sample of stars has a peak at around 300 days, this peak is far more pronounced in the stars with double winds.

3.3. *Infrared Colors*

Figure 4 shows the [12] − [25], [25] − [60], and K − [60] infrared colors for the stars in Table 1, showing the dependence both on profile shape and on chemistry. Here, the colors are referred to those of a 0 mag star, using the zero-point flux densities in the *IRAS* Explanatory Supplement (1988). The 12 μm, 25 μm, and 60 μm flux densities from which these colors are calculated are from the *IRAS* Point Source Catalog, Version 2 (1988) except for the S stars, whose flux densities are given by Jorissen & Knapp (1998). The K-band magnitudes are taken from the compilation by Gezari et al. (1993), from Le Bertre (1992, 1993), and from Kerschbaum & Hron (1994). There may be large uncertainties in these colors, especially in K − [60] because the flux densities are not observed at the same point in the

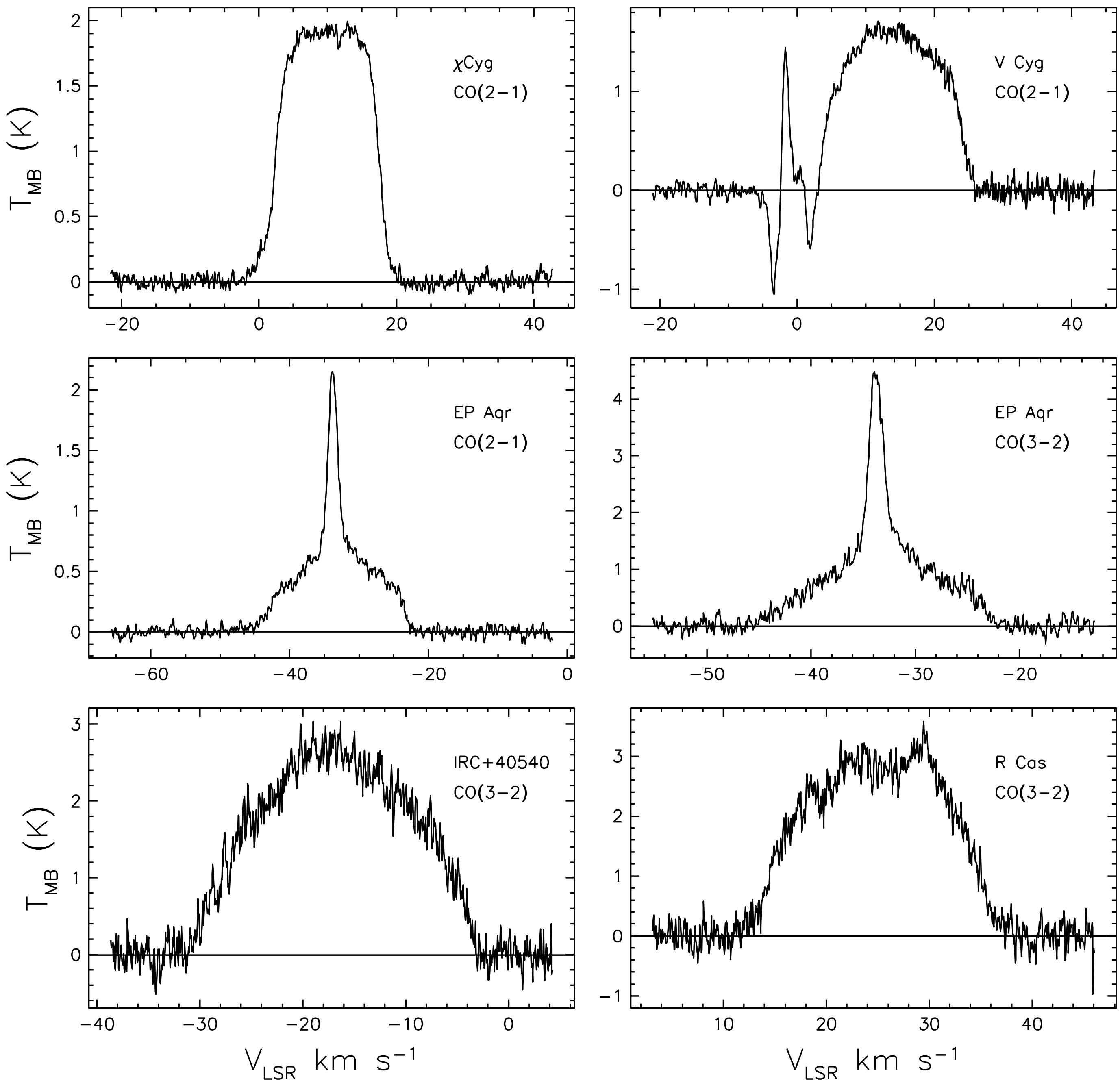

FIG. 1.—*Continued*

star's variability cycle (typically, $\Delta K \sim 1$ mag; Le Bertre 1992). Figures 4*a* and 4*c* show $[25]-[60]$ versus $[12]-[25]$ (cf. van der Veen & Habing 1988) and $K-[60]$ versus $[12]-[25]$, respectively, showing the colors as a function of profile shape, while Figures 4*b* and 4*d* show these relationships as a function of envelope chemistry. Generally, the higher the mass-loss rate, the redder the infrared colors (van der Veen & Habing 1988). Figure 4 shows that stars with double winds are not present in the regions of these color-color diagrams occupied by stars with high mass-loss rates; that this is not simply an artifact of the dependence of infrared color on circumstellar chemistry is shown by comparison with Figures 4*b* and 4*d*.

3.4. *Summary*

Nine of the 45 evolved stars in the sample in Table 1 have double winds, and only one of these is a carbon star. The stars with double winds have infrared colors, which suggest that they have mass-loss rates lying at the low end of those in the sample and also have shorter periods than average. Further, three of the six S stars have double winds. There are two tentative conclusions from these properties: (1) it is unlikely that the double wind phenomenon is the result of binarity, since the frequency of double winds appears to depend on stellar chemistry and variable type, both of which are intrinsic to the star; and (2) they suggest that the

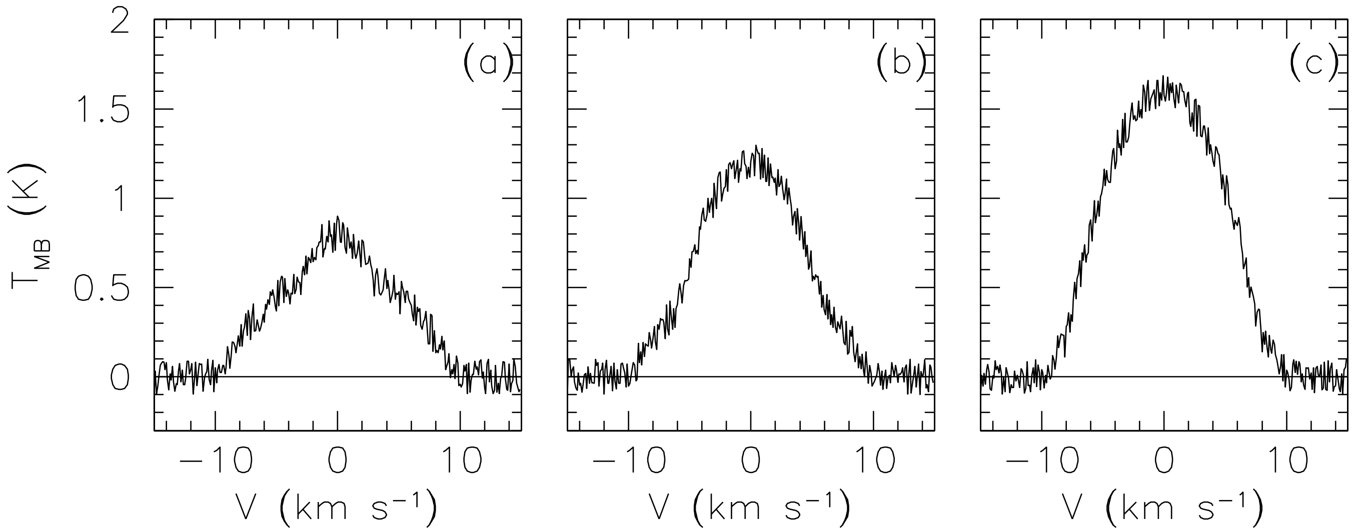

FIG. 2.—Simulated CO(2–1) line profiles as observed with the CSO 10.4 m telescope for stars with double winds. In all cases the faster wind has an outflow speed $V_f = 10$ km s^{-1} and a mass-loss rate of 3×10^{-7} $M_{\odot}$ yr^{-1}. The model star is at a distance of 200 pc. The simulated line profiles have a velocity resolution of 0.1 km s^{-1} and an rms channel-to-channel noise of 0.04 K. The line profile of the fast wind is parabolic with a peak temperature of 0.65 K. (*a*) Outflow speed of slow wind $V_s = 3$ km s^{-1}, peak temperature $T_s = 0.2K$ (5 times the rms noise). (*b*) $V_s = 6$ km s^{-1}, $T_s = 0.6$ K. (*c*) $V_s = 8$ km s^{-1}, $T_s = 1.0$ K.

double-wind phenomenon may be associated with period irregularities and occur when the chemistry and perhaps stellar pulsation and mass loss are undergoing a transition from one phase to another.

4. PHYSICAL PROPERTIES OF THE CIRCUMSTELLAR ENVELOPES

4.1. *Kinematics*

The parameters of the spectral lines, measured from the high velocity resolution profiles, are given in Table 2, which lists for each star the CO transition observed, the rms noise,

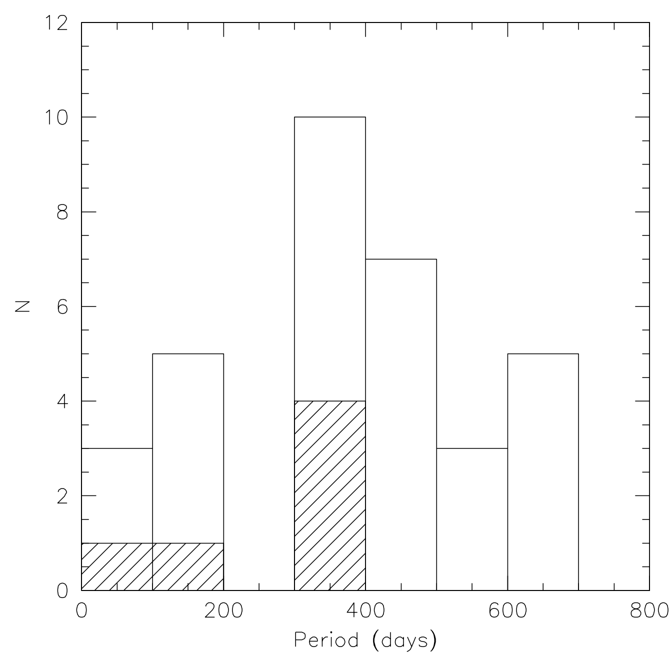

FIG. 3.—Period distribution for the evolved stars in Table 1. *Hatched columns*: stars with double molecular winds.

the integrated CO line intensity I_{CO} in K × km s^{-1}, and the peak line temperature T_{peak}, the central velocity V_c, and the terminal wind outflow velocity V_o. The last three quantities were calculated for most of the line profiles by fitting a flattened parabolic line profile of the form

$$T(V) = T_{peak}\left(1 - \exp\left\{-\alpha\left[1-\left(\frac{V-V_c}{V_o}\right)^2\right]\right\}\right)\Big/(1 - e^{-\alpha}) \tag{1}$$

(Knapp & Morris 1985) to the data. This was also done for the asymmetric line profiles such as that for R Leo to yield average quantities. The line profiles for IRC +60144, AFGL 971, and V Cyg are partly contaminated by galactic emission. Equation (1) was fitted to the uncontaminated regions of the profile, and the integrated line intensity I_{CO} was estimated assuming that the line shape is parabolic: $I_{CO} = 4/3 T_{peak} V_o$. These values are enclosed in parentheses in Table 2.

The line profiles for stars with two components were modeled by a superposition of two parabolas. No fit was made for the CO(2–1) profile for R Hya; this profile is very asymmetric. CO(2–1) data for RS Cnc from Jorissen & Knapp (1998) and CO(3–2) data for *o* Cet from Knapp et al. (1998a) were also analyzed. The profile fits for the stars with double winds are shown in Figure 5. Table 2 lists the parameters for the broad and narrow components separately. As Figure 5 shows, these fits are adequate for most of the stars. The narrow components for several stars appear to be more Gaussian than parabolic in shape. Two stars, *o* Cet and R Hya, have broad components whose redshifted emission is stronger than the blueshifted emission; the profiles for the remaining stars are roughly symmetric.

The central velocities V_c and outflow velocities V_o measured by the CO(2–1) and CO(3–2) lines agree well for the stars for which both lines have been observed. The central velocities of the broad and narrow components are the same to within the errors for all stars, with $\langle V_c$(broad)

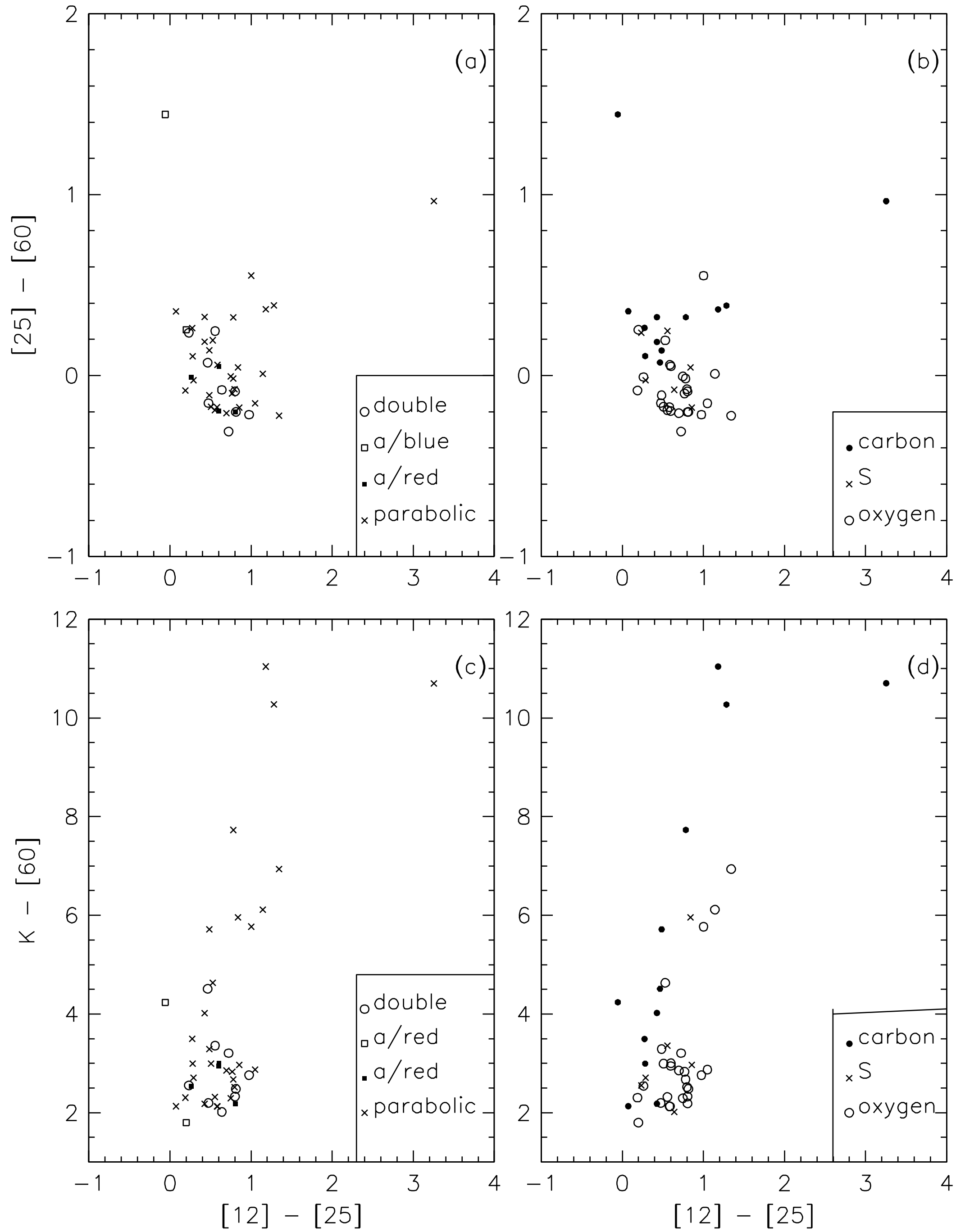

FIG. 4.—[25] − [60] vs. [12] − [25] and K − [60] vs. [12] − [25] color-color diagrams for evolved stars. (*a*), (*c*): Colors as a function of line shape. (*b*), (*d*): Colors as a function of chemistry.

$- V_c(\text{narrow})\rangle = -0.2$ km s^{-1}. Thus both flows are centered on the star (and among other things, this means that it is very unlikely that the narrow components are due to a chance superposition of interstellar emission on the stellar line profile). Figure 6 shows the histograms of the outflow velocities for stars with double winds: the outflow velocities of the broader component are shown in Figure 6*a* and of the narrower component in Figure 6*b*. For comparison, the histogram of outflow speeds for the stars in Table 2 with single winds is shown in Figure 6*c*. Figure 6*c* appears to contain data for a representative sample of stars; the distribution is very similar to that found for other samples (see, e.g., Zuckerman, Dyck, & Claussen 1986). The distributions of outflow velocities in stars with double winds differ from those in stars with single winds (although this difference is subject to the difficulties in distinguishing two components when the outflow velocities have similar values—see the discussion in § 2). The broad components have somewhat larger outflow velocities than typical, but much more striking is the difference between Figures 6*b* and 6*c*; the narrow components have much smaller outflow velocities than average. Figure 6 suggests that the really unusual property of most of the stars with double winds is the presence of a component with a very small outflow speed. (The excep-

TABLE 2

CO LINE PARAMETERS FROM HIGH-VELOCITY RESOLUTION PROFILES

Star	Line	rms	I_{CO}	T_{peak}	V_c	V_o
IRC +40004	2–1	0.064	14.0 ± 2.6	0.51 ± 0.08	−20.5 ± 1.8	19.6 ± 2.4
R And	3–2	0.46	12.8 ± 3.6	1.07 ± 0.63	−15.3 ± 5.4	8.8 ± 4.5
R Scl	2–1	0.017	27.8 ± 0.5	1.01 ± 0.10	−19.0 ± 0.9	16.5 ± 1.1
IRC +50049	2–1	0.055	8.1 ± 1.0	0.50 ± 0.10	−2.5 ± 0.5	9.5 ± 0.5
				0.52 ± 0.08	−1.8 ± 0.2	2.6 ± 0.3
o Cet	3–2	0.23	76.2 ± 3.0	5.8 ± 1.2	+46.0 ± 1.0	6.7 ± 1.0
				9.0 ± 1.4	+46.6 ± 0.2	2.4 ± 0.4
IRC +50096	3–2	0.21	32.8 ± 6.3	1.64 ± 0.25	−16.4 ± 1.6	14.9 ± 2.7
IRC +60144[a]	2–1	0.050	(14.3)	0.45 ± 0.08	−48.0 ± 2.0	20.5 ± 2.1
				0.16 ± 0.06	−45.0 ± 1.5	5.6 ± 2.4
TX Cam	3–2	0.17	32.7 ± 6.5	1.27 ± 0.21	+11.2 ± 2.1	19.0 ± 3.2
R Lep	2–1	0.046	13.2 ± 1.6	0.44 ± 0.06	+12.3 ± 1.2	17.4 ± 1.5
α Ori	2–1	0.039	8.2 ± 1.1	0.32 ± 0.06	+3.4 ± 1.2	14.2 ± 1.2
U Ori	3–2	0.10	7.2 ± 1.5	0.71 ± 0.18	−38.1 ± 1.3	7.5 ± 1.2
AFGL 865	2–1	0.041	16.5 ± 1.4	0.81 ± 0.06	+43.1 ± 0.7	15.3 ± 0.9
AFGL 971[a]	3–2	0.14	(15.4)	0.77 ± 0.19	+3.3 ± 2.9	14.9 ± 5.1
GX Mon	2–1	0.052	22.9 ± 2.0	0.75 ± 0.06	−9.2 ± 1.0	19.5 ± 1.2
R Gem	2–1	0.038	2.68 ± 0.84	0.05 ± 0.02	−59.2 ± 0.7	11.0 ± 1.1
				0.30 ± 0.05	−59.0 ± 0.6	4.8 ± 0.9
HD 56126	2–1	0.048	9.2 ± 0.9	0.64 ± 0.07	+73.0 ± 0.8	10.7 ± 1.1
S CMi	3–2	0.095	1.5 ± 0.6	0.31 ± 0.08	+51.5 ± 1.4	3.3 ± 1.4
RS Cnc	2–1	0.074	12.5 ± 1.2	0.88 ± 0.0.14	+7.5 ± 0.5	8.0 ± 0.5
				1.00 ± 0.13	+7.2 ± 0.2	2.4 ± 0.3
	3–2	0.12	18.0 ± 1.9	1.10 ± 0.2	+7.5 ± 0.3	8.0 ± 0.6
				1.66 ± 0.2	+7.2 ± 0.3	2.8 ± 0.4
R LMi	2–1	0.025	2.72 ± 0.38	0.24 ± 0.06	0.0 ± 0.6	7.8 ± 0.5
IW Hya	3–2	0.122	12.3 ± 3.4	0.61 ± 0.18	+40.4 ± 2.5	13.6 ± 4.1
R Leo	3–2	0.076	21.9 ± 1.2	2.0 ± 0.2	−0.5 ± 0.5	6.8 ± 0.7
IRC +10216	2–1	0.28	424.2 ± 8.3	19.1 ± 0.6	−25.5 ± 0.3	14.6 ± 0.3
U Hya	2–1	0.044	10.0 ± 0.6	0.98 ± 0.10	−30.9 ± 0.4	6.7 ± 0.5
R Crt	2–1	0.050	11.1 ± 1.1	0.59 ± 0.07	+11.2 ± 0.7	10.8 ± 0.7
BK Vir	2–1	0.039	8.4 ± 0.5	0.29 ± 0.05	+17.1 ± 0.8	5.8 ± 1.1
Y UMa	2–1	0.030	3.2 ± 0.3	0.40 ± 0.05	19.0 ± 0.5	5.4 ± 0.6
Y CVn	3–2	0.12	10.7 ± 1.9	0.88 ± 0.17	21.1 ± 0.9	7.8 ± 1.3
RT Vir	2–1	0.023	4.9 ± 0.4	0.37 ± 0.03	+17.5 ± 0.5	8.9 ± 0.6
SW Vir	2–1	0.022	11.7 ± 0.4	0.89 ± 0.11	−11.1 ± 0.6	7.8 ± 0.7
R Hya[b]	2–1	0.022	4.9 ± 0.5			
	3–2	0.10	22.2 ± 2.2	1.2 ± 0.3	−10.0 ± 0.8	11.0 ± 1.2
				0.8 ± 0.2	−9.7 ± 0.6	5.0 ± 0.7
S Vir	2–1	0.025	0.64 ± 0.25	0.09 ± 0.03	+9.8 ± 2.3	5.2 ± 2.2
W Hya	3–2	0.17	28.3 ± 2.7	2.0 ± 0.3	+40.8 ± 0.6	8.1 ± 0.8
RX Boo	3–2	0.15	23.9 ± 2.4	1.65 ± 0.21	+1.5 ± 0.7	9.6 ± 1.0
S CrB	2–1	0.034	2.53 ± 0.51	0.25 ± 0.04	+1.1 ± 0.9	7.4 ± 1.2
V CrB	3–2	0.23	4.3 ± 1.0	0.39 ± 0.08	−99.4 ± 1.3	6.3 ± 1.2
R Ser	3–2	0.17	3.5 ± 1.9	0.52 ± 0.04	+31.6 ± 0.5	5.3 ± 0.9
X Her	2–1	0.026	6.4 ± 0.4	0.38 ± 0.05	−72.8 ± 0.8	8.5 ± 1.0
				0.45 ± 0.07	−73.2 ± 0.4	3.2 ± 0.5
	3–2	0.071	13.3 ± 1.3	0.7 ± 0.1	−73.2 ± 0.5	9.0 ± 1.0
				0.99 ± 0.12	−73.1 ± 0.3	3.5 ± 1.4
RU Her	2–1	0.011	2.3 ± 0.2	0.18 ± 0.03	−12.1 ± 0.8	9.4 ± 1.5
W Aql	2–1	0.030	43.9 ± 1.2	1.63 ± 0.09	−24.1 ± 0.6	17.6 ± 0.8
χ Cyg	2–1	0.038	28.8 ± 0.7	1.98 ± 0.14	+9.9 ± 0.4	8.9 ± 0.5
V Cyg[a]	2–1	0.067	(25.0)	1.61 ± 0.09	+14.0 ± 0.5	11.8 ± 0.6
EP Aqr	2–1	0.035	12.8 ± 0.8	0.70 ± 0.10	−33.0 ± 0.5	10.8 ± 0.8
				1.36 ± 0.21	−33.8 ± 0.2	1.4 ± 0.2
	3–2	0.10	24.3 ± 2.3	1.30 ± 0.3	−33.0 ± 0.5	10.8 ± 1.0
				3.05 ± 0.60	−33.7 ± 0.2	1.5 ± 0.3
π^1 Gru[c]	2–1	...	...	...	−10	27
				...	−13	12
IRC +40540	3–2	0.17	49.8 ± 4.8	2.61 ± 0.26	−16.8 ± 0.9	14.3 ± 1.4
R Cas	3–2	0.20	51.8 ± 4.8	2.94 ± 0.34	+24.9 ± 0.9	12.1 ± 1.2

[a] Contaminated by Galactic emission.
[b] No fit possible.
[c] Data from Sahai 1992 observed with 15 m SEST.

tions are IRC +60144 with $V_s = 5.6$ km s^{-1} and $V_f = 20.5$ km s^{-1}, and π^1 Gru, with $V_S = 12$ km s^{-1} and $V_f = 27$ km s^{-1}.) Indeed, Figure 6 suggests that there are essentially *no* stars with single winds with outflow speeds less than about 3 km s^{-1} and that these low-velocity flows appear only in stars with double winds.

Figure 6*c* also shows the distributions of the wind speeds in stars with double winds, i.e., the sum of the data from Figures 6*a* and 6*b*. The distributions for stars with single winds and with double winds are quite different. This

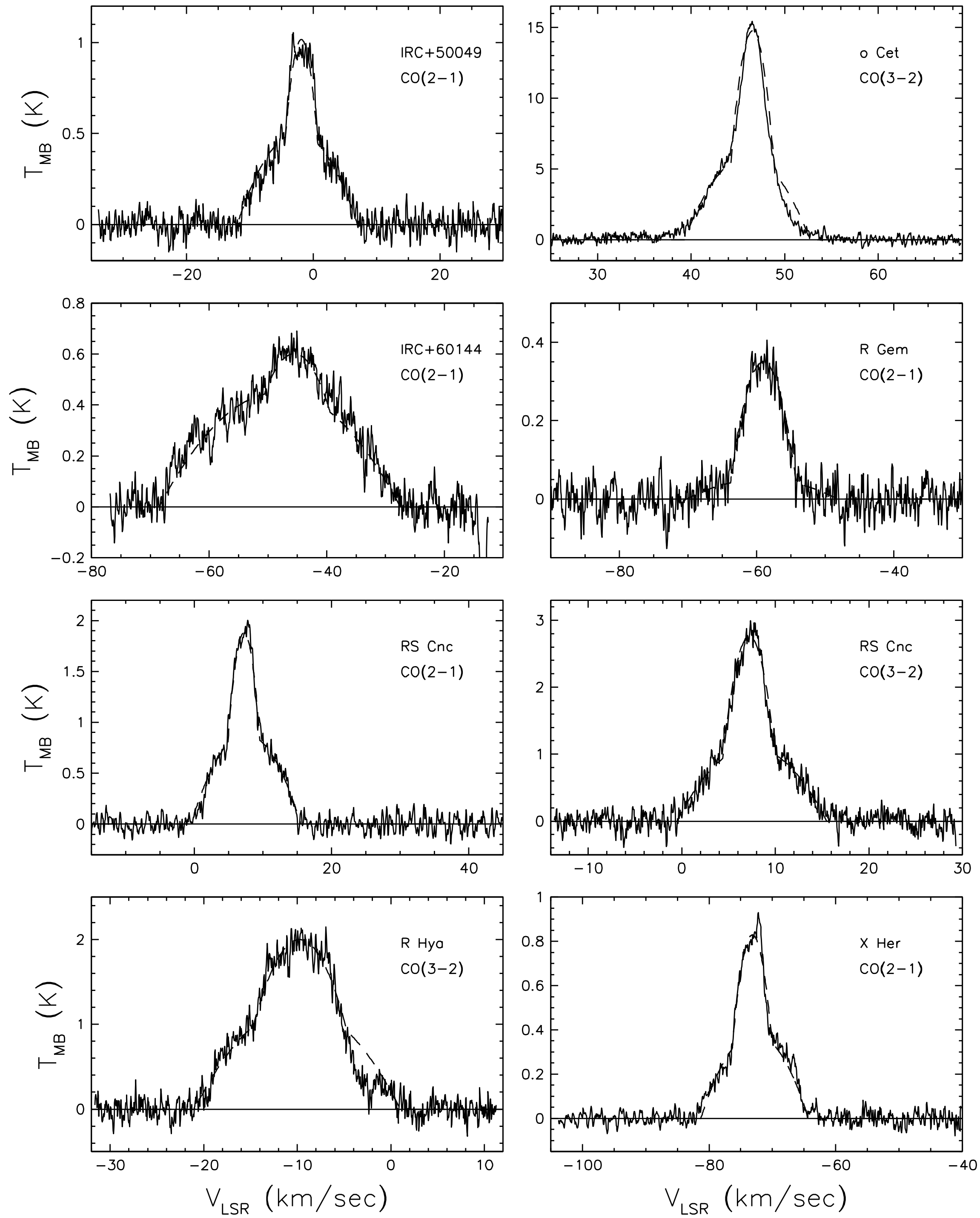

FIG. 5.—CO profiles for stars with double winds showing profile fits (*dashed lines*)

implies that there is indeed an intrinsic difference between the envelopes of stars whose line profiles show one component and those that show two components.

Figure 7 shows the velocity of the slow wind versus that of the fast wind for the nine stars with double winds. With the exception of EP Aqr, the slow and fast wind velocities are proportional to each other.

4.2. *Distances*

In the next section, we model the circumstellar CO emission to derive values for the mass-loss rates. A prerequisite for this modeling is a measurement or estimate of the stellar distance, and this situation has changed dramatically in recent months with the publication of the *Hipparcos* catalog (Perryman et al. 1997—see also van Leeuwen et al. 1997). Thirty-three of the stars in Table 1 are in the *Hipparcos* Main Catalogue, and 23 of these have parallaxes measured at greater than the 2 σ level. The distances to these stars are taken directly from the *Hipparcos* catalog.

Other methods for estimating distances to AGB stars include using a period-M_V or period-M_K relationship; assuming a constant absolute K magnitude; or assuming a constant bolometric luminosity (see, e.g., Claussen et al. 1987; Jura 1988; Young 1995; Knapp et al. 1998b). These

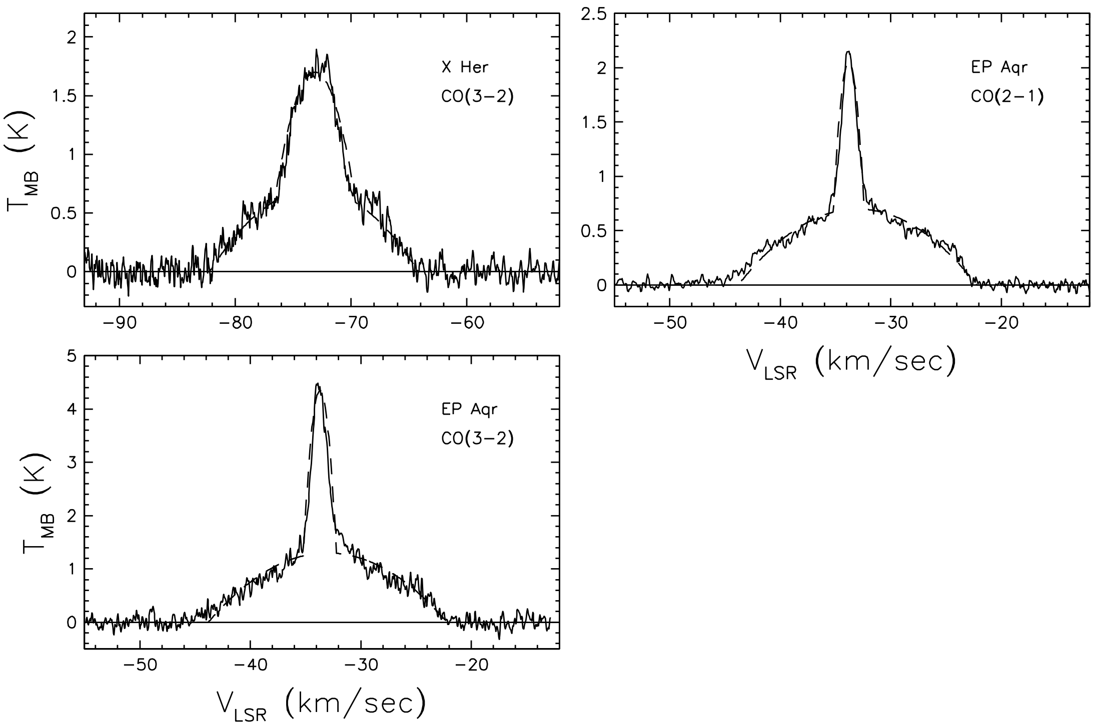

FIG. 5.—*Continued*

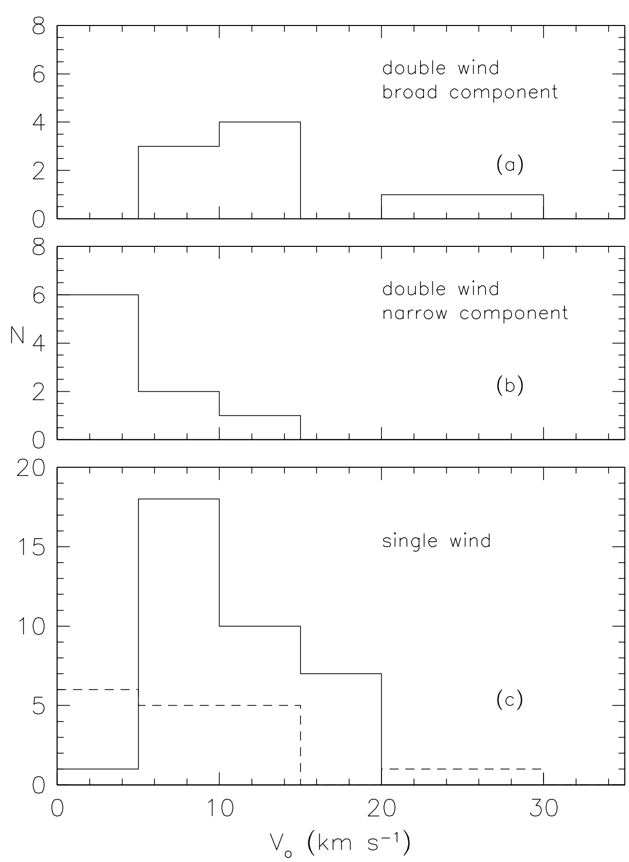

FIG. 6.—Histograms of wind outflow speeds for (*a*) the broad component of stars with double winds, (*b*) the narrow components of stars with double winds, and (*c*) stars with single winds. The summed distributions for the broad and narrow components is shown by dashed lines.

methods can be reevaluated using the *Hipparcos* distances, and a preliminary discussion is given below.

Several studies (e.g., Claussen et al. 1987; Jura 1988; Jorissen & Knapp 1998) have assumed the value of $M_K = -8.1$ mag found for carbon stars in the Magellanic Clouds (Frogel, Persson, & Cohen 1980). The values of M_K for the stars in Table 1 with parallaxes, regardless of chemistry, are

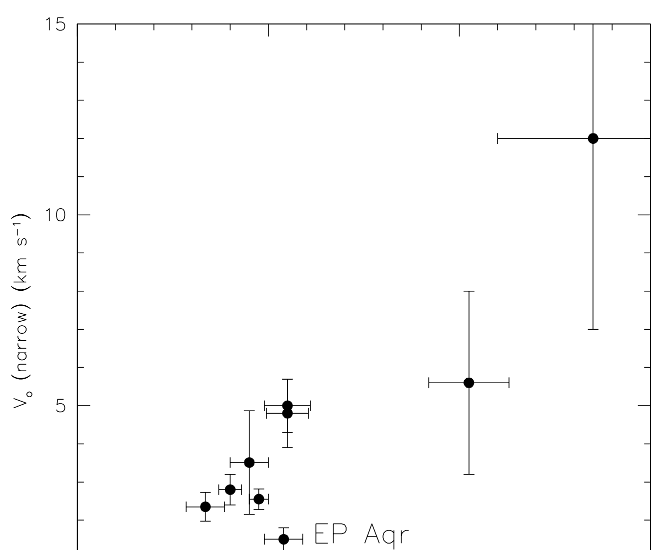

FIG. 7.—Outflow speeds of slow vs. fast winds for nine stars with double winds.

shown in Figure 8*a*. These were calculated from the *K* magnitudes in the compilation of Gezari et al. (1993) and parallaxes from the *Hipparcos* catalog. Apart from the supergiant α Ori ($M_K = -9.6$ mag) the stars appear to have a mean absolute *K* magnitude about 1 mag fainter than -8.1 mag. However, all of these stars are losing mass and so have significant circumstellar extinction. The approximate K extinction was found from

$$A_K = 3 \times 10^7 \dot{M}(M_\odot \ \mathrm{yr}^{-1}) V_o^{-1}(\mathrm{km\ s}^{-1}) + 10^{-4} D(\mathrm{pc}) . \quad (2)$$

The first term is the circumstellar extinction, and the second, the interstellar extinction (with *D* the distance in pc). These quantities were found by assuming a gas-to-extinction ratio $N_\mathrm{H}/A_V = 2 \times 10^{21}$ cm^{-2} mag^{-1} for both the circumstellar and interstellar gas, and an extinction curve with $R = A_V/E_{B-V} = 3.1$, which gives $A_V/A_K = 8.9$. The circumstellar extinction was calculated assuming constant mass-loss rate and outflow velocity, so that $n(r) \sim r^{-2}$, and an inner radius for the dust shell of 5×10^{13} cm. The extinction corrections for the stars in Figure 8*a* were calculated from the mass-loss rates given by the present CO observations (see below), and the resulting distribution of M_K is shown in Figure 8*b*. It should be emphasized that this calculation is very uncertain; the differences between circumstellar and interstellar matter, and between envelopes of different chemical composition, have not been considered; there is growing evidence (see, e.g., recent papers by Skinner et al. 1997 and Whitelock et al. 1997) that AGB mass loss is anisotropic; and the apparent *K* magnitudes are uncertain because of variability (see, e.g., Le Bertre 1992). It is clear from Figure 8*b* that the extinction has been much overestimated for several stars, but the results do support the use of a single absolute *K* magnitude, consistent with the Magellanic Cloud carbon star value of -8.1 mag, for all stars, and show that circumstellar extinction is often significant.

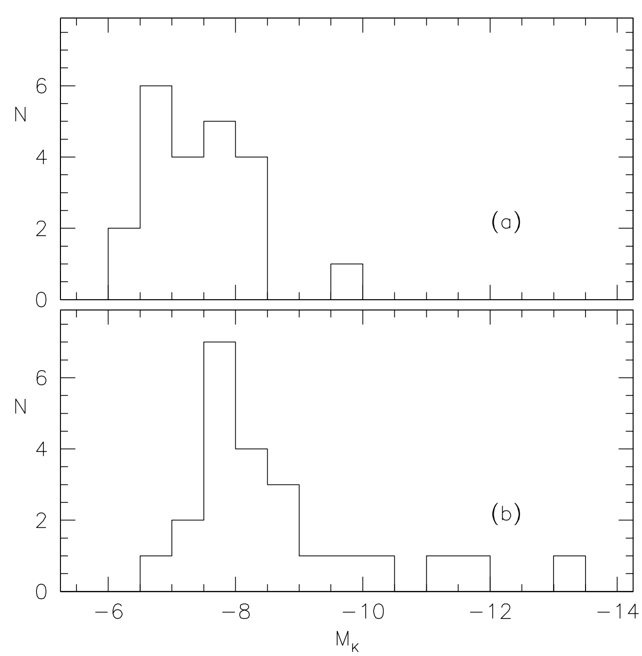

FIG. 8.—Absolute *K* magnitudes for stars with *Hipparcos* parallaxes (*a*) observed and (*b*) corrected for circumstellar and interstellar extinction.

For stars in the present study that do not have *Hipparcos* parallaxes, the distances were found using one or more of the above methods. Stars whose distances were found using $M_K = -8.1$ mag were modeled in an iterative process; a first distance estimate was made, the mass-loss rate was calculated, the circumstellar extinction was calculated, and the distance was reestimated. In all cases, the distance estimates were checked to be sure that they are not discrepant with the lower limits given by *Hipparcos*. These distance estimates are preliminary and should be refined using a larger sample of stars; the absolute magnitudes of carbon and oxygen stars should also be further investigated. Distances were also estimated in some cases using $L_\mathrm{bol} = 10^4$ $L_\odot$. The only serious inconsistency was found for R Hya, whose "*K* magnitude" distance (115 pc) is significantly smaller that the limit of >200–300 pc from the *Hipparcos* parallax—see also van Leeuwen et al. 1997b). No distance estimate was made for the post-AGB star HD 56126.

4.3. *Mass-Loss Rates*

The mass-loss rates were calculated using the model of Morris (1980) and Knapp & Morris (1985) to calculate the emission from a model spherical envelope produced by constant mass loss at constant outflow speed. The envelope radius was assumed to be truncated by photodissociation of CO, using the rates given by Mamon et al. (1988). The CO/H_2 abundance was taken as 5×10^{-4} for oxygen stars, 6.5×10^{-4} for S stars, and 10^{-3} for carbon stars (see Knapp et al. 1998b). The slow and fast components for stars with double winds were treated separately. The results are given in Table 3, which gives for each star the distance, the chemistry, the assumed outflow velocity V_o, the resulting mass-loss rate $\dot{M}$, and the source of the distance. These mass-loss rates generally agree reasonably well with previous estimates—that for IRC +10216, for example, is about a factor of 2 lower than the value found by Crosas & Menten (1997) after the different model abundances are taken into account.

Figure 9 shows histograms of the mass-loss rates for the separate double-wind components: the broad component (Fig. 9*a*) and the narrow component (Fig. 9*b*). For comparison, the distribution for the stars in Table 3 with single winds is shown in Figure 9*c*. The broad components have a distribution similar to that of the stars with single winds; the narrow components have mass-loss rates that are much smaller than typical.

Several authors (e.g., Netzer & Elitzur 1993; Young 1995) have demonstrated an empirical relationship between mass-loss rate $\dot{M}$ and outflow speed V_o for winds from AGB stars that provides a useful method for displaying and comparing data sets. Such a relationship is expected for radiationally driven dusty winds, since the grain-gas coupling becomes less effective for lower mass-loss rates (Gilman 1972; Goldreich & Scoville 1976; Netzer & Elitzur 1993; Ivezic & Elitzur 1995; Crosas & Menten 1997).

The mass-loss rate and outflow speed are plotted against each other in Figures 10–12; these figures show the same data subdivided in several different ways. Figure 10 shows the plot for stars with distances measured by *Hipparcos* and those measured by other means. Both samples show a strong correspondence between $\dot{M}$ and V_o, but Figure 10 raises the interesting possibility that the distances to the stars found to have the highest mass-loss rates (most, though not all, are carbon stars) have been overestimated,

TABLE 3

MASS-LOSS RATES

Star	D(pc)	Chemistry	V_o (km s^{-1})	$\dot{M}$($M_\odot$ yr^{-1})	Distance Method
IRC +40004	850	O	19.6	8.4×10^{-6}	M_K, L_{bol}
R And	490	S	8.8	9.4×10^{-7}	M_K
R Scl	475	C	16.5	2.7×10^{-6}	M_K, *Hipparcos*
IRC +50049	142	O	9.5	1.5×10^{-7}	*Hipparcos*
			2.6	2.7×10^{-8}	
o Cet	128	O	6.7	4.4×10^{-7}	*Hipparcos*
			2.4	9.4×10^{-8}	
IRC +50096	650	C	14.9	4.4×10^{-6}	M_K, L_{bol}
IRC +60144	850	C	20.5	4.8×10^{-6}	M_K, L_{bol}
			5.6	2.4×10^{-7}	
TX Cam	280	O	19.0	2.3×10^{-6}	M_K, L_{bol}
R Lep	250	C	17.4	5.2×10^{-7}	*Hipparcos*
α Ori	131	O	14.2	3.1×10^{-7}	*Hipparcos*
U Ori	300	O	7.5	2.9×10^{-7}	M_K, $P-M_K$, *Hipparcos*
AFGL 865	1800	C	15.3	2.2×10^{-5}	M_K, L_{bol}
AFGL 971	1300	C	14.9	7.6×10^{-6}	M_K, L_{bol}
GX Mon	500	O	19.5	4.8×10^{-6}	M_K, L_{bol}
R Gem	850	S	11.0	4.1×10^{-7}	M_K
			4.8	4.5×10^{-7}	
S CMi	470	O	3.3	6.6×10^{-8}	$P-M_K$; M_K
RS Cnc	122	S	8.0	1.0×10^{-7}	*Hipparcos*
			2.6	2.3×10^{-8}	
R LMi	270	O	7.8	1.6×10^{-7}	$P-M_K$; M_K; *Hipparcos*
IW Hya	900	O	13.6	4.2×10^{-6}	M_K; L_{bol}
R Leo	101	O	6.8	9.4×10^{-8}	*Hipparcos*
IRC +10216	150	C	14.6	9.2×10^{-6}	M_K, L_{bol}
U Hya	162	C	6.7	9.2×10^{-8}	*Hipparcos*
R Crt	300	O	10.8	6.9×10^{-7}	M_K, $P-M_K$, *Hipparcos*
BK Vir	176	O	5.8	6.9×10^{-8}	*Hipparcos*
Y UMa	313	O	5.4	1.7×10^{-7}	*Hipparcos*
Y CVn	218	C	7.8	1.1×10^{-7}	*Hipparcos*
RT Vir	138	O	8.9	1.1×10^{-7}	*Hipparcos*
SW Vir	143	O	7.8	1.7×10^{-7}	*Hipparcos*
R Hya	200	O	11.0	4.7×10^{-7}	M_K; *Hipparcos*
			5.0	7.3×10^{-8}	
S Vir	420	O	5.2	8.4×10^{-8}	*Hipparcos*
W Hya	115	O	8.1	1.7×10^{-7}	*Hipparcos*
RX Boo	156	O	9.6	3.0×10^{-7}	*Hipparcos*
S CrB	400	O	7.4	2.5×10^{-7}	M_K; $P-M_K$; *Hipparcos*
V CrB	600	C	6.3	2.5×10^{-7}	M_K; *Hipparcos*
R Ser	279	O	5.3	9.2×10^{-8}	*Hipparcos*
X Her	138	O	9.0	1.1×10^{-7}	*Hipparcos*
			3.4	3.4×10^{-8}	
RU Her	400	O	9.4	3.2×10^{-7}	M_K; $P-M_K$; *Hipparcos*
W Aql	610	S	17.6	9.4×10^{-6}	M_K
χ Cyg	106	S	9.0	2.3×10^{-7}	*Hipparcos*
V Cyg	271	C	11.8	9.4×10^{-7}	*Hipparcos*
EP Aqr	135	O	10.8	2.3×10^{-7}	*Hipparcos*
			1.4	1.7×10^{-8}	
π^1 Gru	153	S	27	5.7×10^{-7}	*Hipparcos*
			12	4.6×10^{-7}	
IRC +40540	700	C	14.3	7.4×10^{-6}	M_K; L_{bol}
R Cas	107	O	12.1	5.2×10^{-7}	*Hipparcos*

and hence the mass-loss rates have been overestimated: these stars, with $\dot{M} \geq 3 \times 10^{-6}\ M_\odot$, do not have *Hipparcos* parallaxes (they are optically too faint) and lie above the relationship found for the stars which do. This should be further investigated with a larger sample. The stars with *Hipparcos* distances show $\dot{M} \sim V_o^2$, a shallower relationship than that found by Young (1995).

Figure 11 shows the data broken down into single winds, the slow components of double winds, and the fast components. All types of component appear to follow the same relationship between $\dot{M}$ and V_o. Figure 12 shows the data divided by stellar chemistry; all of the stars appear to follow the same relationship.

5. DISCUSSION

The results presented in the previous sections of this paper show that the phenomenon of evolved stars with double winds is quite common: at least 20% of the stars observed with high velocity resolution have two components centered at the same velocity. The present data show that the phenomenon is particularly common in S stars, but this remains to be confirmed by observations of a larger sample. In addition, several stars were found to have strongly asymmetric profiles. These phenomena are almost absent in carbon stars. The tendency of this sort of velocity structure to be found in semiregular variable stars, or stars

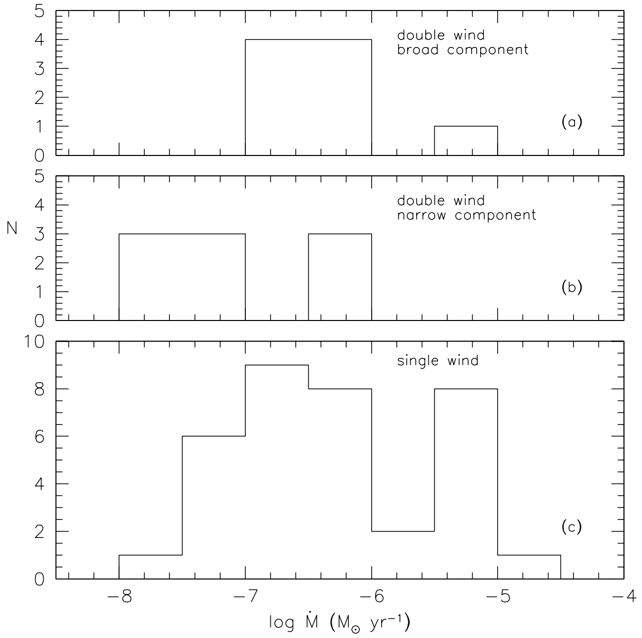

FIG. 9.—Distributions of mass-loss rates for (*a*) broad components and (*b*) narrow components of stars with double winds and (*c*) stars with single winds.

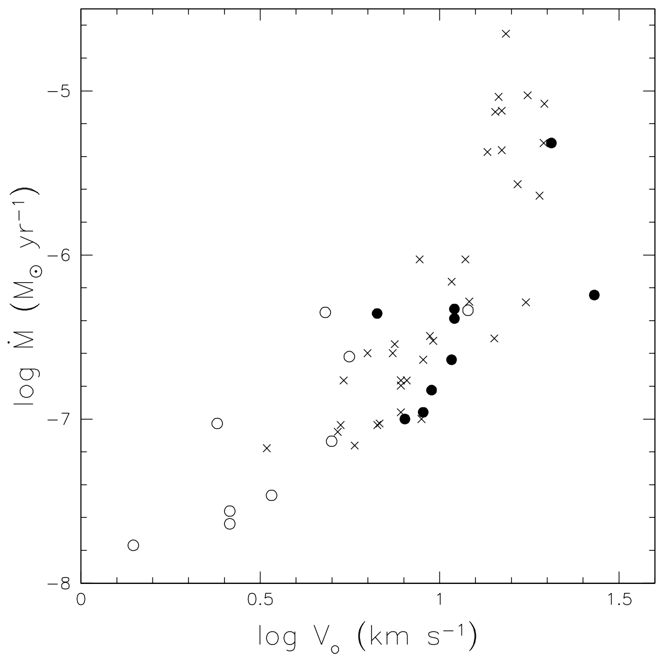

FIG. 11.—Mass-loss rate vs. wind outflow speed. *Filled symbols*: stars with double winds, broad components. *Open symbols*: stars with double winds, narrow components. *Crosses*: stars with single winds.

with short periods, as well as in S stars, suggests that double winds accompany changes in the stellar properties (pulsation mode, period etc.) (see also Olofsson 1997a; Jorissen & Knapp 1998).

If all stars go through one or more stages in which winds at two different velocities are produced, the present data show that they spend at least 20% of their AGB evolution in such a phase. The total lifetime of stars in the mass-losing phase on the AGB has been estimated at $\sim 2 \times 10^5$ yr (see, e.g., Young, Phillips, & Knapp 1993a, 1993b), so that stars would spend $\sim 4 \times 10^4$ yr in a phase or phases in which two winds are produced.

Studies of Mira variables have found a correlation between pulsation period and mass-loss rate (see, e.g., Jura 1988; van der Veen & Habing 1988), and between period and wind outflow speed (Dickinson & Chaisson 1973), which demonstrates the role of pulsation in mass loss. Semi-regular variables, which generally have shorter pulsation periods, do not show a period-velocity correlation (Dickinson & Dinger 1982). Figures 13 and 14 show these relationships for stars in the present sample whose periods are known (Table 1), sorted by variable type. The period–

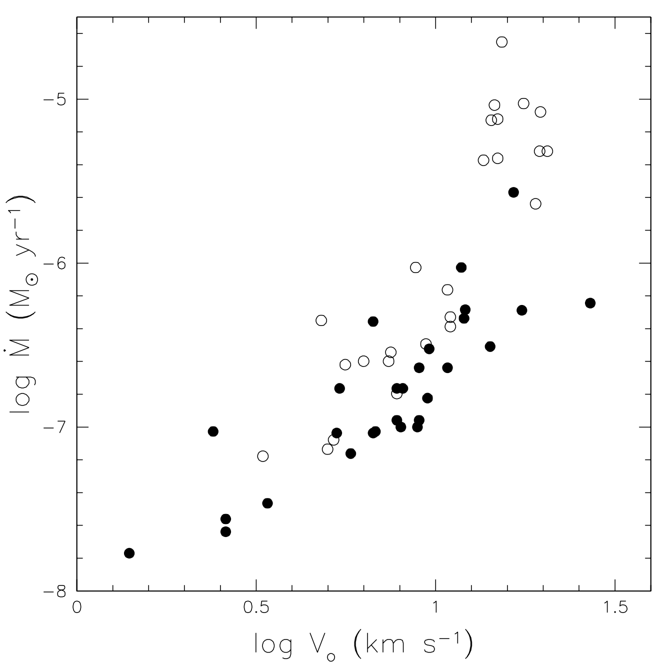

FIG. 10.—Mass-loss rate vs. wind outflow speed. *Filled symbols*: stars with *Hipparcos* parallaxes. *Open symbols*: distances derived by other methods (see text).

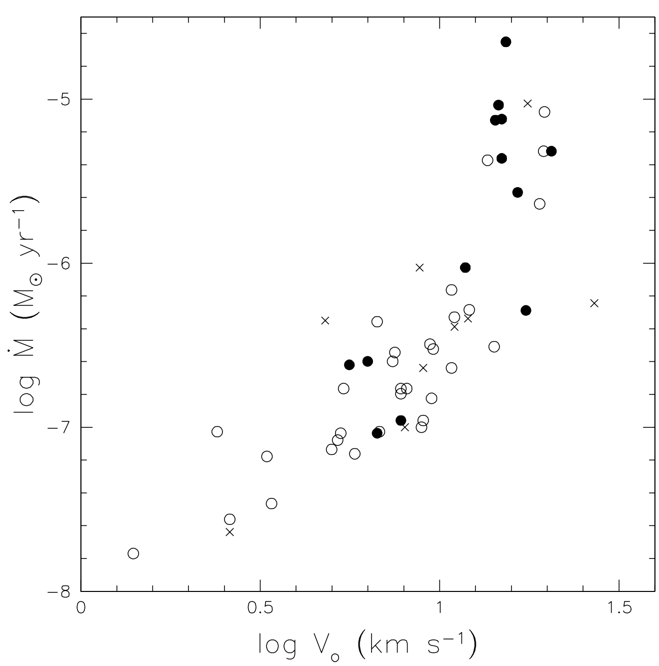

FIG. 12.—Mass-loss rate vs. wind outflow speed. *Filled symbols*: carbon stars. *Open symbols*: oxygen stars. *Crosses*: S stars.

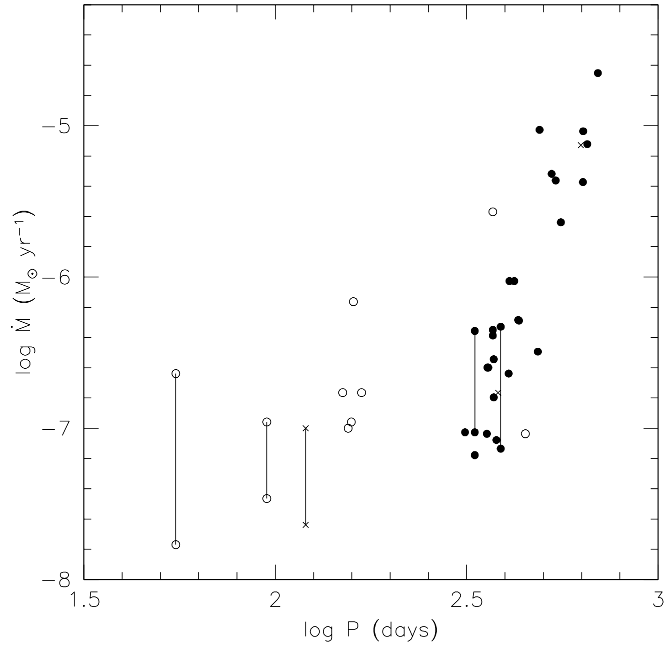

FIG. 13.—Mass-loss rate in $M_\odot$ yr^{-1} vs. s pulsation period (days) for stars with measured periods (Table 1), sorted by variable type. *Filled symbols*: Mira variables. *Open symbols*: SRb variables. *Crosses*: SRa, SRc, and unknown type. The data for α Ori (SRb: $P = 2070$ days) are not plotted. Vertical lines join the mass-loss rates for stars with double winds.

mass-loss rate correlation for Mira variables in Figure 13 and the period–outflow velocity correlation for Mira variables in Figure 14 are fairly well defined but are not followed by the semiregular variables, as found by Dickinson & Dinger (1982). The data for Mira variables with double winds shown in these figures suggest that the considerable scatter in these relationships may be intrinsic and that the stellar properties (luminosity, period etc.) do not uniquely determine the mass-loss rate.

As the data discussed in this paper have shown, it is the slow winds that are unusual; they have outflow speeds and mass-loss rates far lower than typical for evolved stars. Further, as Figures 7, 13, and 14 show, both the slow and fast winds are related to each other and to the stellar properties. Most of the stars with double winds have fairly low mass-loss rates. As a result, the CO-emitting extent of the circumstellar envelope, determined by photodissociation, is small. Table 4 lists the photodissociation radii R_p for both the slow and fast winds for the stars with double winds; these were calculated using the results of Mamon et al. (1988) as the radii at which the relative CO abundance has decreased to half of its original value. Table 4 also gives the crossing time $T = R_p/V_o$ for both fast and slow winds. If the double-line profiles are due to the cessation of mass loss at one outflow velocity/mass-loss rate and its resumption at a different outflow velocity/mass-loss rate, these times are upper limits to the time interval that can elapse between the cessation of mass loss and its resumption. For several stars (e.g., RS Cnc), this interval is <1000 yr, far shorter than the approximately 5000 yrs observed for some carbon stars with detached circumstellar envelopes (see, e.g., Olofsson et al. 1996; Lindqvist et al. 1996).

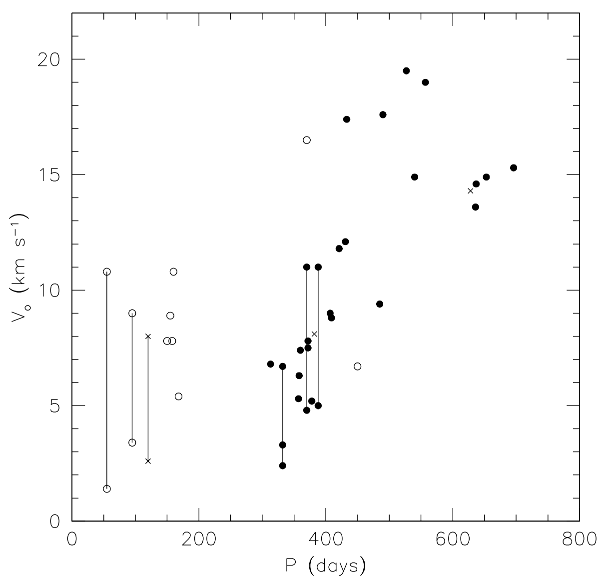

FIG. 14.—Wind outflow speed V_o in km s^{-1} vs. pulsation period (days) for stars with measured periods (Table 1), sorted by variable type. *Filled symbols*: Mira variables. *Open symbols*: SRb variables. *Crosses*: SRa, SRc, and unknown type. The data for α Ori (SRb: $P = 2070$ days) are not plotted. Vertical lines join the velocities for stars with double winds.

TABLE 4

PHOTODISSOCIATION RADII OF STARS WITH DOUBLE WINDS

Star	V_o (km s^{-1})	R_p (cm)	T (yr)
o Cet	6.7	3.8×10^{16}	1800
	2.4	2.4×10^{16}	3100
IRC +60144	20.5	1.4×10^{17}	2170
	5.6	1.7×10^{17}	9700
R Gem	11.0	3.5×10^{16}	1000
	4.8	5.2×10^{16}	3390
RS Cnc	8.0	1.8×10^{16}	710
	2.6	1.1×10^{16}	1370
R Hya	11.0	3.3×10^{16}	950
	5.0	6.0×10^{16}	3750
X Her	9.0	1.7×10^{16}	580
	3.4	1.1×10^{16}	1050
EP Aqr	10.8	2.3×10^{16}	670
	1.4	1.1×10^{16}	2390
π^1 Gru	27	3.6×10^{16}	420
	12	3.6×10^{16}	950

However, the correspondence between the presence of discernible double winds and stellar period, variability, type, and mass-loss rate suggest that the phenomenon occurs only at particular stages in a star's evolution. By analogy with carbon stars with detached envelopes, where the observations show that mass loss has resumed at a much lower mass-loss rate and outflow speed (Olofsson et al. 1996; Lindqvist et al. 1996), and because winds with very low velocities ($V_o \leq 3$ km s^{-1}) seem to occur only in stars with double winds, we tentatively conclude that oxygen and S stars also undergo episodes of interrupted mass loss and that the slow winds represent its resumption.

The present observations add to the growing body of data that shows that the kinematics of circumstellar envelopes are a lot more complex that they appear at first, that changes in the stellar variability modes may produce abrupt changes in the mass-loss rate, and that these changes are fairly common. Future papers in this series will discuss further survey observations, the systematics of slow and fast winds, asymmetric profiles, the relationship to the detached shells seen in some carbon stars (Olofsson et al. 1996), and individual stars in detail.

6. CONCLUSIONS

The CO(2–1) or CO(3–2) line profiles from 43 nearby AGB stars with bright CO emission were measured with high velocity resolution and sensitivity and were combined with observations of two more such stars from the literature. We found the following:

1. At least one-third of the line profiles are strongly nonparabolic in shape. Six stars have asymmetric lines with bright spikes at the red or blue extrema of the profile, and nine have double profiles, i.e., two roughly parabolic lines of different width centered at the same velocity.

2. The stars with nonparabolic profiles have lower pulsation periods and bluer infrared colors (indicating lower mass-loss rates) and are much more likely to be semiregular variables than most of the stars in the sample. Only two of the carbon stars (15%) have nonparabolic profiles, half of the S stars do, and 40% of the oxygen stars. These results suggest that complex winds, whose presence is shown by complex line profiles, occur when the star is undergoing a change in luminosity, pulsation mode, or chemistry.

3. The broad and narrow components of the stars with double winds, analyzed separately, follow the same mass-loss rate/period/outflow velocity relationships as do the stars with parabolic profiles. The broad components have mass-loss rates and outflow velocities typical of mass-losing AGB stars, but the narrow components have far lower velocities and mass-loss rates than are seen in any other sample of evolved mass-losing AGB stars. The narrow components may be due to the resumption of mass loss after it has been stopped by some change in the stellar properties.

4. Comparison of the line widths of ^{29}SiO(8–7) (for oxygen stars) or CS(7–6) (for carbon stars) with the CO(3–2) line widths shows that the SiO/CS lines are systematically narrower than the CO line for stars with $V_o \leq 10$ km s^{-1}; above this velocity, the line widths are roughly equal. These data suggest that the winds in stars with low mass-loss rates do not reach their terminal velocities until relatively large distances, several $\times 10^{15}$ cm.

5. A search for very broad line wings in this sample of stars, like those associated with post-AGB stars (for example, AFGL 618), proved negative except (tentatively) in two stars, where it need further observations. The phenomenon of fast winds appears to be confined to stars that are evolving away from the AGB.

It was a privilege to use the *Hipparcos* database, and we would like to express our appreciation to the *Hipparcos* team for making it so openly available. We thank the staff at CSO, especially Antony Schinkel, Maren Purves, and Tom Phillips, for their support of the observations and the referee, Kay Justtanont, for a prompt and helpful reading of the paper. Astronomical research at the CSO is supported by the National Science Foundation via grant AST96-15025. This research made use of the SIMBAD data base, operated at CDS, Strasbourg, France. Support for this work from Princeton University and from the NSF via grant AST 96-18503 is gratefully acknowledged.

APPENDIX A

A SEARCH FOR FAST ($V_o \geq 50$ km s^{-1}) MOLECULAR WINDS

A small number of evolved stars have very fast ($V_o \geq 50$ km s^{-1}) molecular winds in addition to the slow ($V_o \leq 20$ km s^{-1}) "steady" winds. These winds, some with speeds in excess of 200 km s^{-1}, have, to date, been found in stars that are evolving away from the AGB. There is evidence that the formation of fast winds occurs after that of slow winds and that these fast winds are bipolar (Morris et al. 1987; Cernicharo et al. 1989; Gammie et al. 1989; Bachiller et al. 1991; Neri et al. 1992; Young et al. 1992; Jaminet et al. 1992; Bujarrabal, Fuente, & Omont 1994; Alcolea, Bujarrabal, & Sánchez Contreras 1996; Knapp et al. 1997).

The observations described in the present paper are sensitive enough, and almost always have sufficiently flat baselines, that the line profiles measured with the 500 MHz AOS provide useful information on the presence or absence of very fast winds. As a guide, CSO observations of AFGL 618 find that the ratio of the line brightness temperatures of the fast and "steady" winds is ~ 0.04 for the CO(2–1) line and 0.09 for the CO(3–2) line (Gammie et al. 1989), where the temperature of the fast wind emission is measured at ± 50 km s^{-1} from the central velocity. (The difference in these ratios is probably due to the fast wind being confined to the inner regions of the AFGL 618 circumstellar envelope, while the envelope produced by the steady wind is more extended and is partly resolved.) CSO observations of AFGL 2688 give ratios of about ~ 0.12 and 0.24 (Young et al. 1992), and of V Hya, ~ 0.07 and 0.06 (Knapp, Jorissen, & Young 1997).

However, a word of caution is in order here—the observations in this paper give information only on the fast wind *emission* from evolved stars. Sahai & Nyman (1997) describe their beautiful observations of the "Boomerang" bipolar nebula in the CO(1–0) line where a fast wind is seen in absorption against the microwave background; the wind is presumed to be cooled by rapid adiabatic expansion to a temperature < 3 K. Gas at this temperature has negligible excitation of the CO rotational lines so is not detectable in absorption or emission in any line except CO(1–0).

The 500 MHz filterbank observations of the stars listed in Table 1 were reduced and calibrated as described in § 2, and the reduced profiles were binned to a resolution of ~ 7 km s^{-1} and examined to see if high-velocity emission was present. The results are given in Table 5. The only two stars with any hint of such emission are R Lep and RX Boo, whose CO line profiles are shown in Figure 15; these stars should be reobserved, since this structure could be due to weak emission lines from other molecules in the circumstellar envelope. The CO(2–1) profile of IRC $+10216$ has weak high-velocity wings, with T(wing)/T(peak) ~ 0.0048—see Table 5. However, this feature is almost certainly instrumental; the frequency calibration comb, as measured by the AOS, shows wings at about this level (Table 5). This represents the real limit to the measurable brightness of broad-wing emission.

Otherwise, no high-velocity emission is present for any of the other stars. Table 5 lists the 5 σ upper limit on the brightness temperature of fast wind emission and its ratio to the peak temperature of the steady wind, also taken from the binned

TABLE 5

SEARCH FOR FAST MOLECULAR WINDS IN OBSERVED STARS

Star	Line	T (fast)[a]	R[b]
IRC +40004	2–1	<0.015	<0.028
R And	3–2	<0.12	<0.12
IRC +50049	2–1	<0.01	<0.02
IRC +50096	3–2	<0.04	<0.09
IRC +60144	2–1	<0.015	<0.03
TX Cam	3–2	<0.05	<0.04
R Lep	2–1	(0.02)	(0.05)
α Ori	2–1	<0.01	<0.03
U Ori	3–2	<0.03	<0.04
AFGL 865	2–1	<0.015	<0.02
AFGL 971	3–2	<0.04	<0.05
GX Mon	2–1	<0.015	<0.02
R Gem	2–1	<0.01	<0.05
HD 56126	2–1	<0.01	<0.02
S CMi	3–2	<0.03	<0.2
RS Cnc	2–1	<0.03	<0.02
RS Cnc	3–2	<0.03	<0.02
R LMi	2–1	<0.01	<0.04
IW Hya	3–2	<0.025	<0.04
R Leo	3–2	<0.025	<0.01
IRC +10216	2–1	(0.1)	(0.0048)[c]
U Hya	2–1	<0.01	<0.01
R Crt	2–1	<0.01	<0.02
BK Vir	2–1	<0.01	<0.06
Y UMa	2–1	<0.015	<0.06
Y CVn	3–2	<0.03	<0.04
RT Vir	2–1	<0.02	<0.062
SW Vir	2–1	<0.02	<0.026
R Hya	2–1	<0.02	<0.06
R Hya	3–2	<0.035	<0.02
S Vir	2–1	<0.01	<0.13
W Hya	3–2	<0.03	<0.02
RX Boo	3–2	(0.05)	(0.03)
S CrB	2–1	<0.02	<0.10
V CrB	3–2	<0.06	<0.14
R Ser	3–2	<0.03	<0.07
X Her	2–1	<0.03	<0.06
X Her	3–2	<0.03	<0.02
RU Her	2–1	<0.01	<0.06
W Aql	2–1	<0.03	<0.017
χ Cyg	2–1	<0.02	<0.009
V Cyg	2–1	<0.06	<0.031
EP Aqr	2–1	<0.02	<0.022
IRC +40540	3–2	<0.03	<0.01
R Cas	3–2	<0.04	≪0.01
AOS comb	...	...	0.0061

[a] Brightness temperature of fast wind.

[b] Ratio of brightness temperatures of fast and steady wind. Doubtful values in parentheses.

[c] Wings on the strong emission line are likely to be instrumental—compare the data for the AOS frequency calibration comb.

profiles. Broadband data are not available for a small number of stars because the baselines are nonlinear. The ratios in Table 5 are less than those typically observed in stars with fast winds (see above) for the large majority of the stars. Almost all of these stars have late spectral types, which shows that they are still on the AGB. The single exception is HD 56126, whose spectral type is F5 Iab and which is probably a post-AGB star (van Winckel, Waelkens, & Waters 1996; Justtanont et al. 1996; van Winckel 1997). These data provide additional evidence (subject to the possible existence of cold, fast winds discussed above) that the stage at which fast molecular winds are produced is short-lived and occurs at an evolutionary stage beyond the AGB.

APPENDIX B

COMPARISON OF SiO/CS AND CO OUTFLOW VELOCITIES

The broadband (500 MHz) CO(3–2) observations detected emission from the CS(7–6) line from carbon stars or the ^{29}SiO(8–7) line from oxygen stars in the image sideband: the rest frequencies of these lines are 342.883 GHz and 342.979 GHz,

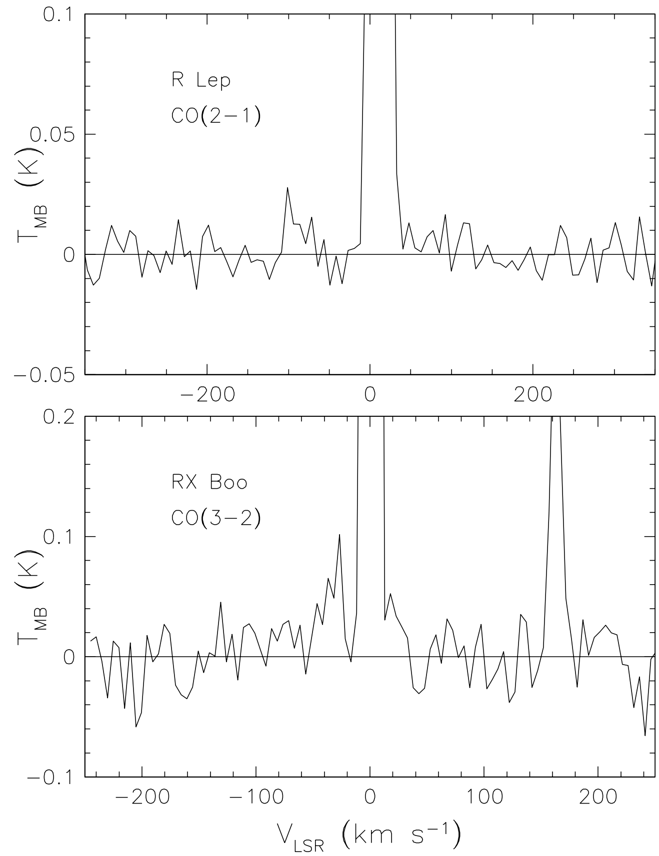

FIG. 15.—CO line profiles, binned to a resolution of ~ 7 km s^{-1}, for (*a*) R Lep and (*b*) RX Boo

respectively. Five of the carbon stars and seven of the oxygen stars have emission of sufficient strength in these lines to allow a comparison of the line widths. The outflow speeds V_o were calculated by fitting a parabolic line to the CS/SiO and CO line profiles. Note that at the approximately 1 km s^{-1} resolution of the 500 MHz AOS, any structure in the line profiles is not resolved and the fitted outflow velocities are likely to find an average of the slow and fast wind velocities.

The results are listed in Table 6, which gives the values for V_o for the CO(3–2) and ^{29}SiO or CS lines calculated from the 500 MHz line profiles, plus the profile classifications and the CO outflow velocities from the 50 MHz observations (see § 4).

Comparison of the CO velocities measured with the 500 MHz and the 50 MHz AOS spectrometers shows the effect of velocity resolution; the lines are broadened by about 1 km s^{-1}. However, the high-resolution CO lines are broader than the

TABLE 6

WIND VELOCITIES IN THE CO(3–2), CS(7–6), AND ^{29}SiO(8–7) LINES

A. Carbon Stars

Star	V_o (CO 3–2)	V_o (CS 7–6)	Profile	V_o (CO 3–2) 50 MHz
IRC +50096......	15.2 ± 0.7	13.7 ± 1.5	P	14.9 ± 2.7
AFGL 971	15.3 ± 0.8	14.4 ± 4.4	(P)	14.9 ± 5.1
Y CVn............	8.7 ± 0.6	7.2 ± 2.2	P	7.8 ± 1.3
V CrB	8.0 ± 1.5	3.9 ± 0.9	(P)	6.3 ± 1.2
IRC +40540......	14.7 ± 0.5	15.7 ± 1.6	P	14.3 ± 1.4

B. Oxygen Stars

Star	V_o (CO 3–2)	V_o [^{29}SiO(8–7)]	Profile	V_o (CO 3–2) 50 MHz
U Ori.............	7.8 ± 1.0	5.6 ± 1.7	P	7.5 ± 1.2
RS Cnc...........	6.4 ± 1.7	4.2 ± 0.2	D	8.0 ± 0.6
				2.8 ± 0.4
R Leo.............	7.7 ± 0.1	4.7 ± 0.7	A/Red	6.8 ± 0.7
R Hya	8.9 ± 1.5	3.7 ± 1.7	D	11.0 ± 1.2
				5.0 ± 0.7
RX Boo	10.0 ± 0.5	7.1 ± 1.1	P	9.6 ± 1.0
X Her.............	7.3 ± 1.9	5.7 ± 1.1	D	9.0 ± 1.0
				3.5 ± 1.4
R Cas.............	12.6 ± 0.6	5.2 ± 1.0	A/Red	12.1 ± 1.2

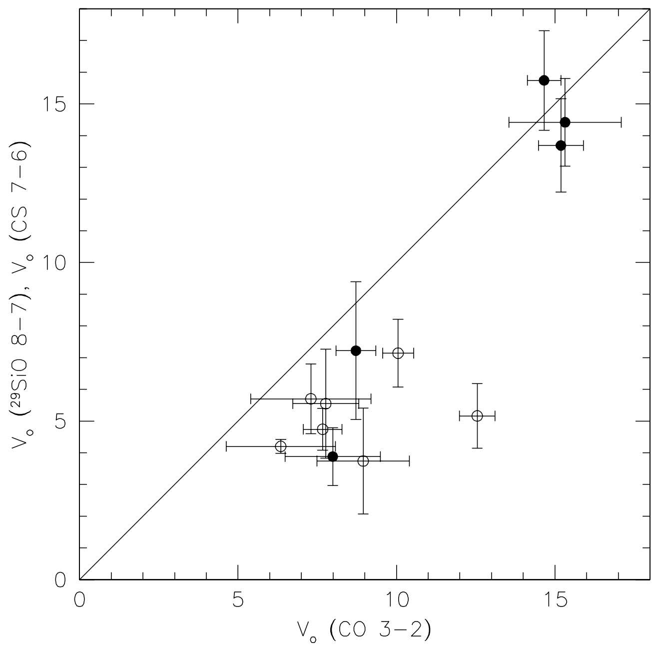

FIG. 16.—Wind outflow speed measured from the CO(3–2) line vs. that measured from the ^{29}SiO(8–7) line (oxygen stars, *open symbols*) or the CS(7–6) line (carbon stars, *filled symbols*).

CS/^{29}SiO lines, which shows that the velocity differences in the second and third columns of Table 6 are real. Three of the stars in Table 6, RS Cnc, R Hya, and X Her, have double winds; the data tentatively suggest that both the slow and fast winds contribute to the ^{29}SiO emission for RS Cnc and X Her and that the ^{29}SiO emission arises only from the slow wind in R Hya. This question should be reexamined with higher velocity resolution observations of the CS and SiO line profiles.

Figure 16 shows the CS/SiO velocity versus the CO velocity for this sample of 12 stars. Overall, the CO lines are slightly broader than the CS/SiO lines, which is probably due to radiative transfer effects in the more extended CO envelope. Additionally, the stars fall into two groups: three carbon stars with V_o(CO) = V_o(CS) and $V_o > 10$ km s^{-1}, and the remaining nine stars in which V_o(CS, SiO) < V_o(CO) and $V_o < 10$ km s^{-1}. The second group contains both carbon and oxygen stars and stars with both parabolic and double line profiles.

CO is abundant and has effective self-shielding against photodestruction; further, its rotational levels are relatively easily excited. ^{29}SiO and CS have much lower abundances and also need higher densities to produce significant rotational line emission; accordingly, the CO emission preferentially measures gas at much larger distances from the star than do lines of less abundant molecules. In these stars, then, the dense gas in the inner regions of the envelope, which gives rise to the CS and ^{29}SiO lines, may not yet be accelerated to the terminal velocity. The results in Figure 16 suggest that the winds from these circumstellar envelopes do not reach their terminal outflow velocity until distances of a few $\times$ 10^{15} cm from the star.

REFERENCES

Alcolea, J., Bujarrabal, V., & Sánchez Contreras, C. 1996, A&A, 312, 560
Bachiller, R., Huggins, P. J., Cox, P., & Forveille, T. 1991, A&A, 247, 525
Bujarrabal, V., Fuente, A., & Omont, A. 1994, ApJ, 421, L47
Cernicharo, J., Guélin, M., Peñalver, J., Martín-Pintado, J., & Mauersberger, R. 1989, A&A, 222, L1
Claussen, M. J., Kleinmann, S. G., Joyce, R. R., & Jura, M. 1987, ApJS, 65, 385
Cohen, M., & Hitchon, K. 1996, AJ, 111, 962
Crosas, M., & Menten, K. 1997, ApJ, 483, 913
Dickinson, D. F., & Chaisson, E. J. 1973, ApJ, 181, L135
Dickinson, D. F., & Dinger, A. S. C. 1982, ApJ, 254, 136
Frogel, J. A., Persson, S. E., & Cohen, J. G. 1980, ApJ, 239, 495
Gammie, C. F., Knapp, G. R., Young, K., Phillips, T. G., & Falgarone, E. 1989, ApJ, 345, L87
Gezari, D. Y., Schmitz, M., Pitts, P. S., & Mead, J. M. 1993, Catalogue of Infrared Observations (NASA Reference Publication 1294)
Gilman, R. S. 1972, ApJ, 178, 423
Goldreich, P. G., & Scoville, N. Z. 1976, ApJ, 205, 144
Groenewegen, M. A. T. 1994, A&A, 290, 531
Habing, H. J. 1996, A&A Rev., 7, 97
Huggins, P. J., & Healy, A. P. 1986, ApJ, 304, 418
IRAS Catalogs and Atlases: Explanatory Supplement. 1988, ed. C. A. Beichman, G. Neugebauer, H. J. Habing, P. E. Clegg, & T. J. Chester (Washington, DC: GPO)
IRAS Point Source Catalog, Version 2, 1988, Joint *IRAS* Science Working Group (Washington, DC: GPO)
Ivezic, Z., & Elitzur, M. 1995, ApJ, 445, 415
Izumiura, H., Hashimoto, O., Kawara, K., Yamamura, I., & Waters, L. B. F. M. 1996, A&A, 315, L221
Jaminet, P. A., Danchi, W. C., Sandell, G., & Sutton, E. C. 1992, ApJ, 400, 535
Jones, T. J., Bryja, C. O., Gehrz, R. D., Harrison, T. E., Johnson, J. J., Klebe, D. I., & Lawrence, G. F. 1990, ApJS, 74, 785
Jorissen, A., & Knapp, G. R. 1998, A&AS, 129, 363
Jura, M. 1988, ApJS, 66, 33
Justtanont, K., Barlow, M. J., Skinner, C. J., Roche, P. F., Aitken, D. K., & Smith, C. H. 1996, A&A, 309, 612
Kahane, C., & Jura, M. 1996, A&A, 310, 952
Kastner, J. H. 1992, ApJ, 401, 337
Kerschbaum, F., & Hron, J. 1992, A&A, 263, 97
———. 1994, A&AS, 106, 397
Kerschbaum, F., Lazaro, C., & Harbison, P. 1996, A&AS, 118, 397
Kholopov, P. N., et al. 1985, General Catalogue of Variable Stars (Moscow: Nauka)
Knapp, G. R., Jorissen, A., & Young, K. 1997, A&A, 326, 318
Knapp, G. R., & Morris, M. 1985, ApJ, 292, 640
Knapp, G. R., Stanek, K. Z., Bowers, P. F., Young, K., & Phillips, T. G. 1998a, in preparation
Knapp, G. R., Woodhams, M. D., Gammie, C. F., Young, K., & Phillips, T. G. 1998b, in preparation
Knapp, G. R., Young, K., & Sahai, R. 1998c, in preparation
Le Bertre, T. 1992, A&AS, 94, 377
———. 1993, A&AS, 97, 729
Lèbre, A., Mauron, N., Gillett, D., & Barthès, D. 1996, A&A, 310, 923
Lindqvist, M., Lucas, R., Olofsson, H., Omont, A., Eriksson, K., & Gustafsson, B. 1996, A&A, 305, L57
Loup, C., Forveille, T., Omont, A., & Paul, J. F. 1993, A&AS, 99, 291
Mamon, G. A., Glassgold, A. E., & Huggins, P. J. 1988, ApJ, 328, 797

Margulis, M., van Blerkom, D. J., Snell, R. L., & Kleinmann, S. G. 1990, ApJ, 361, 673
Morris, M. 1980, ApJ, 236, 823
Morris, M., Guilloteau, S., Lucas, R., & Omont, A. 1987, ApJ, 321, 888
Neri, R., Garcia-Burillo, S., Guélin, M., Cernicharo, J., Guilloteau, S., & Lucas, R. 1992, A&A, 262, 544
Neri, R., Kahane, C., Lucas, R., Bujarrabal, V., & Loup, C. 1997, A&A, in press
Netzer, N., & Elitzur, M. 1993, ApJ, 410, 701
Nyman, L. A., et al. 1992, A&AS, 93, 121
Olofsson, H. 1996, Ap&SS, 245, 169
———. 1997a, in IAU Symp. 177, The Carbon Star Phenomenon, ed. R. F. Wing (Dordrecht: Kluwer), in press
———. 1997b, in IAU Symp. 178, Molecules in Astrophysics: Probes and Processes (Dordrecht: Kluwer), in press
Olofsson, H., Bergman, P., Eriksson, K., & Gustafsson, B. 1996, A&A, 311, 587
Perryman, M. A. C., et al. 1997, A&A, 323, L49
Planesas, P., Bachiller, R., Martín-Pintado, J., & Bujarrabal, V. 1990a, ApJ, 351, 263
Planesas, P., Kenney, J. D. P., & Bachiller, R. 1990b, ApJ, 364, L9
Sahai, R. 1992, A&A, 253, L33
Sahai, R., & Liechti, S. 1995, A&A, 293, 198
Sahai, R., & Nyman, L.-Å. 1997, ApJ, 487, L155
Skinner, C. J., Dougherty, S. M., Meixner, M., Bode, M. F., Davis, R. J., Drake, S. A., Arens, J. F., & Jernigan, J. G. 1997, MNRAS, 288, 295
van der Veen, W. E. C. J., & Habing, H. J. 1988, A&A, 194, 125
van Leeuwen, F., Feast, M. W., Whitelock, P. A., & Yudin, B. 1997, MNRAS, 287, 955
van Winckel, H. 1997, A&A, 319, 561
van Winckel, H., Waelkens, C., & Waters, L. B. F. M. 1996, A&A, 306, L37
Waters, L. B. F. M., Loup, C., Kester, D. J. M., Bontekoe, Tj. R., & de Jong, T. 1994, A&A, 281, L1
Whitelock, P. A., Feast, M. W., Marang, F., & Overbeek, M. D. 1997, MNRAS, 288, 512
Yamamura, I., Shibata, K. M., Kasuga, T., & Deguchi, S. 1994, ApJ, 427, 406
Young, K. 1995, ApJ, 445, 872
Young, K., Phillips, T. G., & Knapp, G. R. 1993a, ApJS, 86, 517
———. 1993b, ApJ, 409, 725
Young, K., Serabyn, G., Phillips, T. G., Knapp, G. R., Güsten, R., & Schulz, A. 1992, ApJ, 385, 265
Zuckerman, B., Dyck, H. M., & Claussen, M. J. 1986, ApJ, 304, 401